Constraints on accretion-ejection structures in young stars

Sylvie Cabrit

Observatoire de Paris

Abstract

This lecture reviews current observational constraints on theoretical models of accretion-driven ejection in young stars. Fundamental properties of jets (collimation scale, kinematics, variability, density, composition) and ejection/accretion ratios are presented and compared at various stages of star formation (Class 0,I,II). Mass-loss rate derivations and evidence for a broader wind component around the jet are also critically examined.

In 1980, Snell et al. reported the discovery in CO of a large **molecular outflow** in the dark cloud L1551. It exhibited a striking bipolar morphology, with well separated lobes of blueshifted and redshifted gas. Within the blue lobe, of typical velocity 15 km s^{-1}, were two previously known Herbig-Haro nebulae with high proper motions of 150 km s^{-1}, pointing away from a position midway between the blue- and red CO lobes. Based on these data, Snell et al. (1980) proposed that the outflow traces ambient gas swept-out into a dense, slow bipolar shell by a fast stellar wind, collimated by a circumstellar accretion disk (see Figure 1).

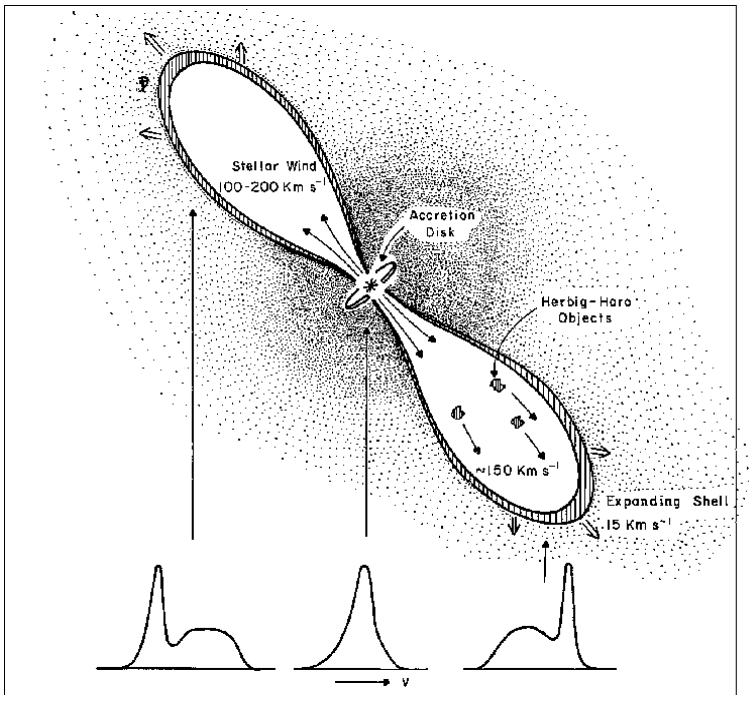

Figure 1: Paradigm proposed by Snell et al. (1980) for the origin of bipolar molecular outflows. Typical CO line profiles from the red and blue CO lobes are sketched at the bottom.

A few years after Snell et al. (1980), the first **jets** were discovered emanating from young stars — including IRS 5, at the center of the L1551 outflow — in optical lines (Mundt & Fried 1983) and in the radio continuum (Bieging, Cohen, & Schwartz 1984). They confirmed that young stars are ejecting matter in an incredibly energetic fashion, but suggested a much higher degree of collimation than initially envisioned.

Two decades later, extensive data has been accumulated on molecular outflows and jets. Although it was totally unanticipated by theories of star formation, jets have turned out to be present in *all* young stellar objects where accretion and/or infall is occuring (see contribution by André, this volume, for a detailed description of these various stages):

- the youngest embedded protostars, with strong infall (Class 0) of ages $\leq 10^4$ yr

- infrared sources with residual infall (Class I), of ages $\simeq 10^5$ yr

- pre-main sequence stars with accretion disks (Class II) of ages $\simeq 10^6$ yr.

How does ejection affect the star, the internal structure of accretion disks, and the initial conditions for planet formation ? The answer to this key question lies in the nature of the ejection mechanism, and in its exact launching zone. Both are still heavily debated and the subject of intense research. One important clue is that, while accretion/infall strongly decreases over time (cf. André's lecture in this volume), ejection and accretion/infall remain closely correlated with one another. This correlation has been a key motivation for the development of MHD models of accretion-ejection structures, which are discussed in detail in Jonathan Ferreira's lecture.

In this contribution, I will review the most recent and quantitative *observational constraints* on accretion-ejection structures in YSOs, that any theoretical model should attempt to satisfy. I first compare fundamental ejection properties in young stars of Class 0,I,II: Tracers, morphology and collimation scale (Section 2), kinematics and variability timescales (Section 3), density and excitation conditions (Section 4). I then review in detail the methods and uncertainties of mass-loss rate derivations from direct jet observation (Section 5), and from observations of swept-up gas in the associated molecular outflows (Section 6), and present the resulting ejection/accretion correlations (Section 7). I finally discuss tentative evidence for a broader wind component surrounding the visible jet (Section 8), and conclude in Section 9.

This lecture, geared towards theoreticians or researchers not already familiar with the field, concentrates on the most solid and general results. For a more in depth coverage of current issues in this rich subject, the reader is referred to the proceedings of the Cozumel meeting (Lizano & Torrelles 1995) and the IAU Symposium No. 182 (Reipurth & Bertout 1997), and to the excellent review of Reipurth & Bally (2001). Theoretical models of jet propagation and shock physics are reviewed in Reipurth & Raga (1999) and Hartigan et al. (2000). Specific reviews on molecular outflows include Lada (1985), Bachiller & Tafalla (1999), and Richer et al. (2000).

1 Jet morphology and collimation scale

1.1 Jet tracers and morphology in the various stages

Despite their widely different tracers, reviewed below, jets appear to have surprisingly similar morphologies in the three evolutionary stages of accreting young stars, namely: a narrow inner beam with knot spacing of 500-1000 AU that can be traced out to 0.1pc from the central source,

and a series of individual, aligned shocked structures with spacing 0.05-0.2 pc, extending up to several parsecs from the source. The origin of such knotty structure will be discussed together with jet kinematics in Section 3.

- *In Class 0 sources*, collimated jets were first resolved by the VLA at centimeter wavelengths. These small-scale **radio jets** trace thermal free-free continuum (bremstrahlung) from ionized gas within 100 AU of the star (see e.g. Rodriguez 1995 and Anglada 1996 for reviews). No optical jet counterparts have yet been detected, either because they are intrinsically faint, or because of the very large $A_v > 1000$ towards these dust-enshrouded protostars. In contrast, distinctive signatures of highly collimated mass-loss are seen in molecular lines:

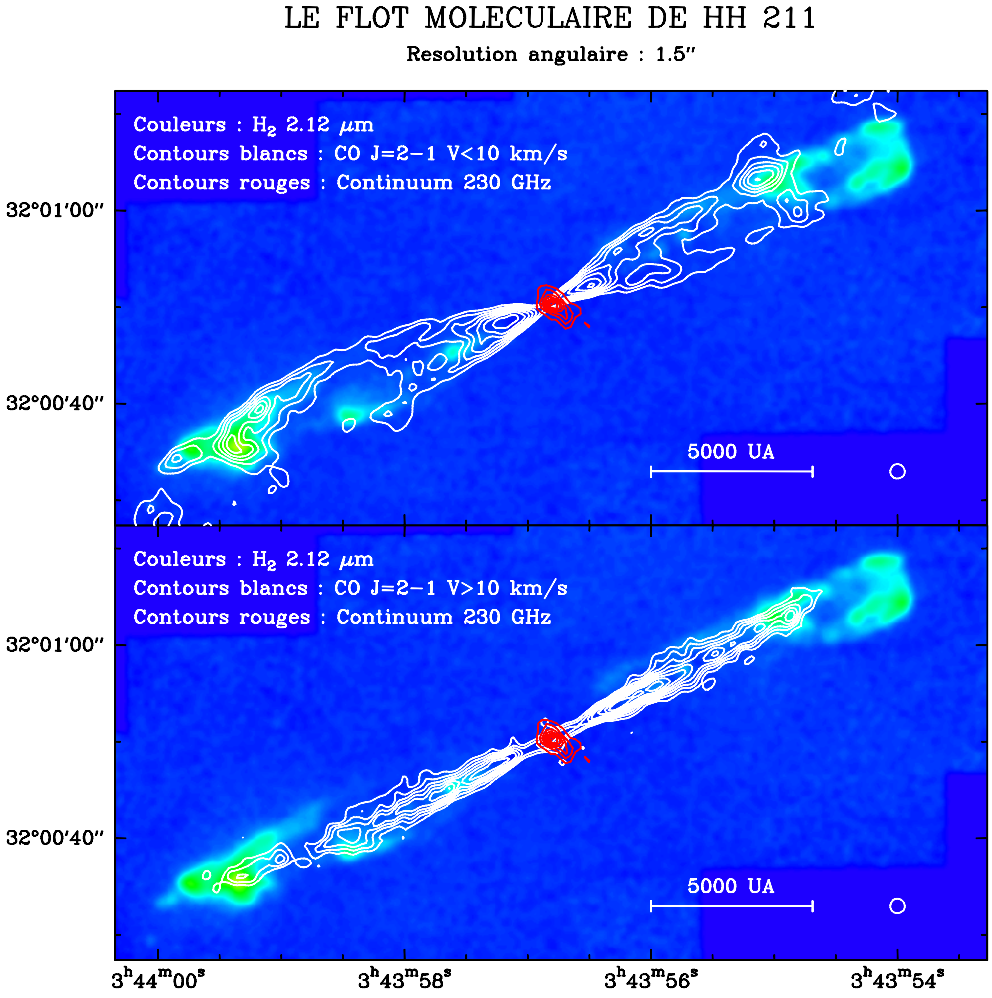

Figure 2: Bipolar molecular flow (top) and molecular jet (bottom) in the Class 0 source associated with HH 211. Contours of CO(2-1) emission (Gueth & Guilloteau 1999) are superposed on a color image in H_2 at 2.12μm (McCaughrean et al. 1994) tracing warm shock-excited gas.

Within 100 AU of the source, 40% of the Class 0 objects excite H_2O masers tracing very dense shocks, some with a highly bipolar structure (Furuya et al. 2001 and refs. therein; Chernin 1995). Narrow **molecular jets** extending to 0.05-0.1 pc from the source have been resolved in CO and SiO lines with mm interferometers in a few cases. They have a knotty morphology, with a typical knot spacing of 1000 AU (Guilloteau et al. 1992; Gueth & Guilloteau 1999; Chandler & Richer 2001). Figure 2 shows the very young molecular jet in the $10 L_\odot$ Class 0 source HH 211. A fine example of molecular jet in a high-luminosity Class 0 source is IRAS 20126+4104 (Cesaroni et al. 1999). Further out, 0.1-1pc along the slow molecular

outflow axis, chains of compact, fast **molecular bullets** are detected, often associated with shock-excited regions in the rovibrational $v = 1-0$ S(1) line of H_2 at 2.12μm (see e.g. Bachiller et al. 1990; Bally, Lada, & Lane 1993). The bullets tend to be regularly spaced, with a typical separation of 0.05-0.2pc. The spatial relationship between these various tracers is illustrated in Figure 3 in the case of the L 1448 outflow.

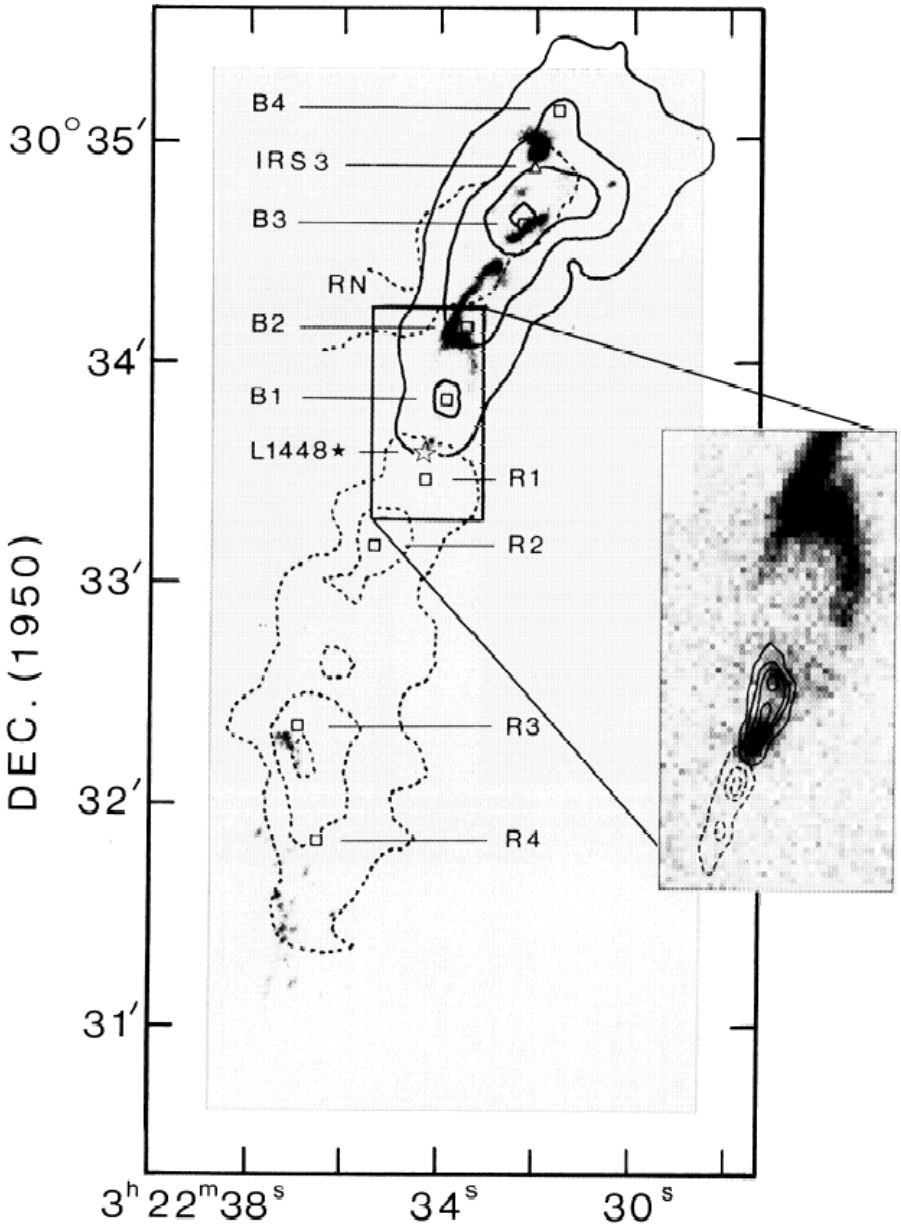

Figure 3: Molecular jet, fast bullets, and slow swept-up outflow in L 1448 (d=300 pc). Contours of CO(2-1) intensity in the low-velocity outflow are superposed on a greyscale image of H_2 2.12μm emission. The positions of SiO and CO bullets B1-B4 and R1-R4 are denoted by open squares. The insert shows the inner SiO jet (contours) superposed on the H_2 image (greyscale). From Bally, Lada, & Lane (1993).

- *in Class I sources*, radio jets are still seen, but shock-excited H_2 and molecular outflows are fainter than in the Class 0 stage. Extended jets become optically visible in lines such as Hα, [O I]λ6300, [S II]λ6731,λ6716, and [N II]λ6583, typical of atomic shock waves of speed 20-150 km s^{-1}. The [Fe II] near-infrared lines are also a very useful tracer, less subject to extinction.

The jet morphology is illustrated in Figure 4, which shows optical Hubble Space Telescope images of the best studied, brightest three cases, HH 111, HH 47, and HH 34 (Reipurth et al. 1997b).

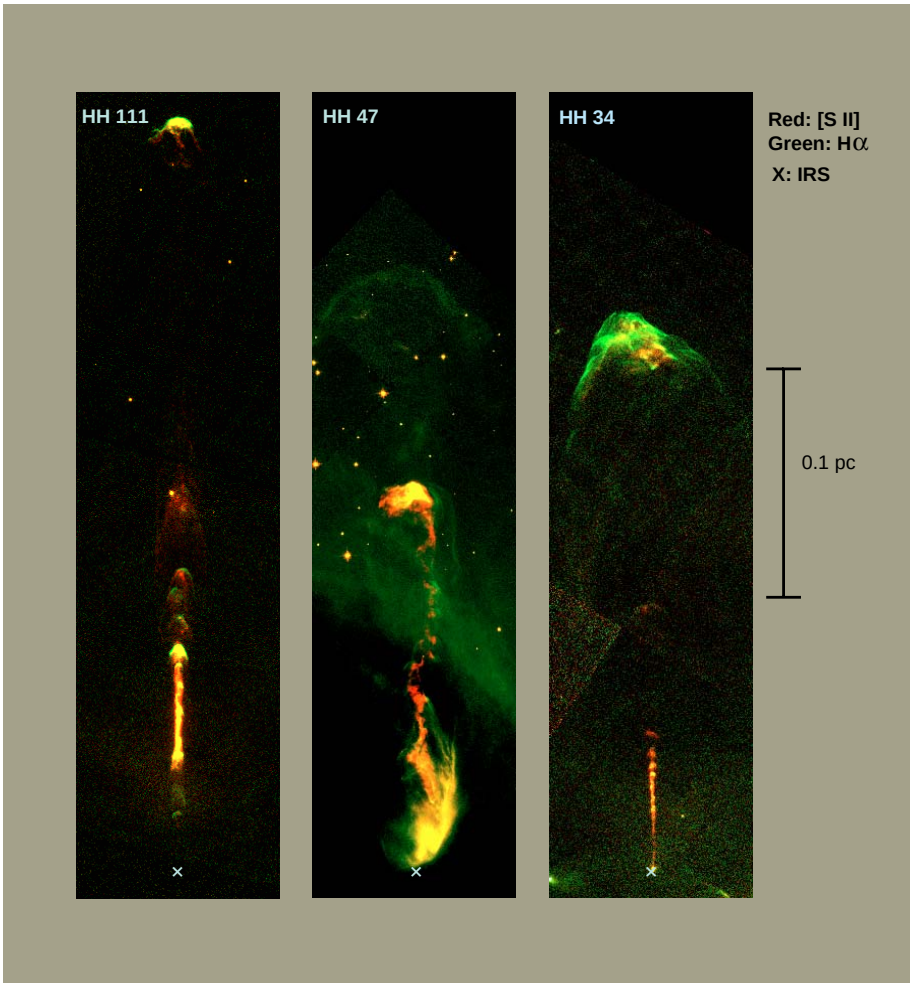

Figure 4: HST images of 3 bright jets from Class I sources on the same linear scale, from the detailed comparative study of Reipurth et al. (1997b). Note that the whole HH 211 molecular flow/jet of Fig.2 would fit in the gap between the source and optically visible jet section in HH 111

The narrow jet beam can be traced out to $\leq$ 0.1pc from the central source, and contains small bright knots with separations of a few arcseconds ($\simeq$ 500-1000 AU). After the jet beam has faded, one finds individual bright, large bow-shaped structures, their apex facing away from the source (see Fig. 4). They belong to the class of **Herbig-Haro [HH] objects**, discovered in the 1950s and characterized by a shock emission line spectrum. In more embedded sources, similar bow shaped structures are seen in shock-excited H_2 (HH 211; see Fig. 2) and are also cataloged as HH objects, by extension (Reipurth 2001: `http://www.casa.colorado.edu/hhcat`).

In several Class I sources, successive optical or H_2 bows have been traced well beyond the inner jet beam, with a typical spacing between bows of 0.05-0.2pc. Spectacular examples are the HH 34 and the HH 111 **parsec-scale jets**, which extend up to 1.5-3.5 pc on either side of the central source (Devine et al. 1997; Reipurth, Bally, Devine 1997a). This discovery has considerably lengthened estimated jet dynamical ages ($\simeq 5 \times 10^4$ yrs for superjets, instead of 300-3000 yrs for the inner jet section), thus reconciling them with the statistical duration of

the Class I phase. The importance of parsec-scale jets for star formation and cloud evolution is reviewed by Reipurth & Bally (2001).

- *in Class II sources*, the presence of atomic collimated winds is indicated by blueshifted forbidden lines of [O I]λ6300, [S II]λ6731, and [N II]λ6583 in the stellar spectrum (Appenzeller et al. 1984; Edwards et al. 1987). Faint radio jets and molecular outflows are only present in the most extreme sources (on the border with Class I). H_2 emission is not detectable anymore. Most of the forbidden line flux arises on small scales < 100 AU that are heavily confused by the much brighter stellar photosphere. Careful subtraction of the stellar continuum using long-slit spectroscopy at various angles reveals high-velocity collimated **microjets** extended over a few 100 AU in 30% of the T Tauri stars studied (Solf 1989; Hirth et al. 1997 and references therein). In the remaining 70% of the sample, microjets are either absent or just too cold to emit. Jets are similarly found in higher mass analogs of T Tauri stars: the Herbig Ae/Be stars (see Mundt & Ray 1994; Corcoran & Ray 1998a).

Sub-arcsecond imaging of microjets has been recently achieved through integral field spectroscopy or adaptive optics or with HST (Lavalley et al. 1997; Lavalley-Fouquet et al. 2000; Dougados et al. 2000; Bacciotti et al. 2000; Reipurth et al. 1998). The jet beam also has a knotty morphology, with a typical knot spacing of 500AU. More distant, faint knots are sometimes detected out to 0.1pc, but no parsec-scale jets have yet been identified at this evolutionary stage. If they exist they must be fainter than in the Class I stage. Figure 5 shows the morphology and proper motions of the bright microjet from the T Tauri star DG Tau.

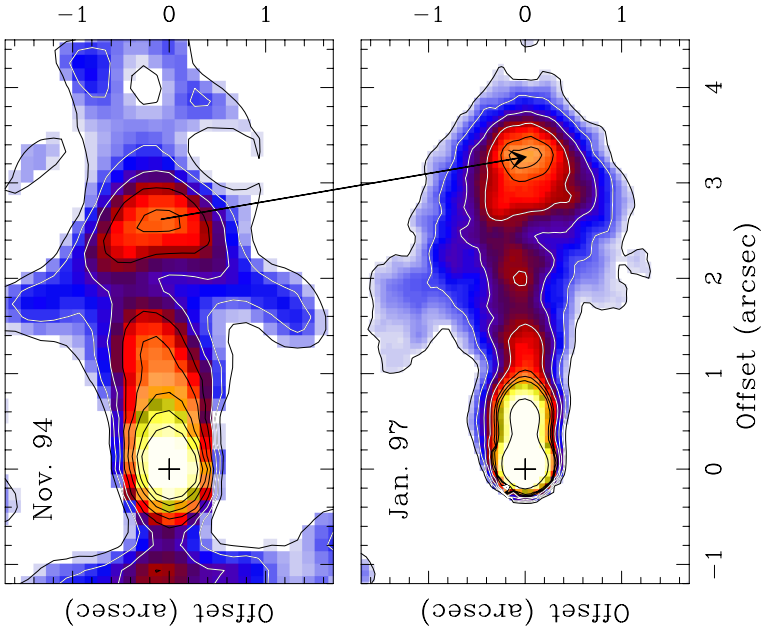

Figure 5: [O I]λ6300 images of the microjet from the Class II T Tauri star DG Tau (1 arcsecond = 140 AU). Note the two bright knots at 0.6" and 3" from the star. A proper motion of 200 km s^{-1} is measured for the outer knot between the two epochs, suggesting an "ejection date" of 1985. From Dougados et al. 2000

1.2 Inner jet width and collimation

- *Optical jets:* The most stringent constraints on collimation scale come from measurements of jet widths within 800 AU of the star in nearby Class II sources in the Taurus cloud (140 pc),

with HST and ground-based adaptive optics (Ray et al. 1996; Dougados et al. 2000). Current results are summarized in Figure 6. Jets appear resolved transversely and collimated as close as 35-50 AU from the central star, with a characteristic width of 30 AU and an opening angle of a few degrees. If the jet originates from a region within 1 AU of the star, it must have a much larger initial opening angle $\geq 45^o$ to reach the observed width, and then undergo strong recollimation *within 35-50 AU* of the source. Further out, the jet width increases slowly to $\simeq$ 70 AU at $d = 800$ AU. Both the widths and small opening angles match up well with the larger scale behavior of Class I jets, studied at $d \geq 1000$ AU (Mundt et al. 1991; Ray et al. 1996; Reipurth et al. 2000a).

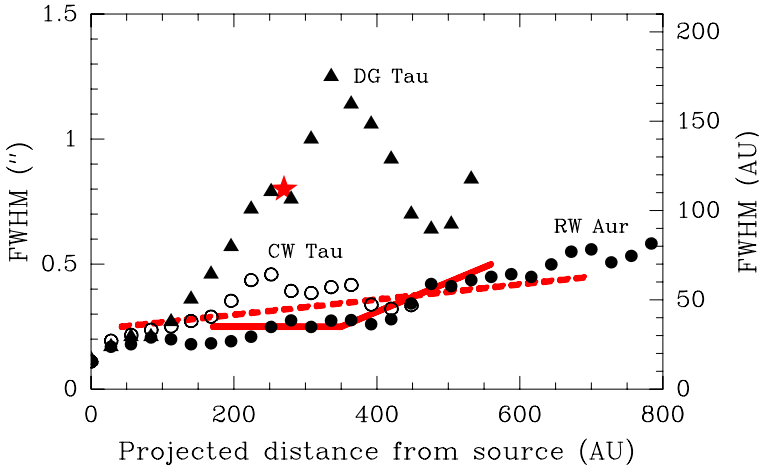

Figure 6: Optical jet widths within 800 AU of the star. Symbols show T Tauri microjets resolved with adaptive optics. HST measurements from Ray et al. (1996) are plotted as a dashed curve (HH 30), solid curve (HL Tau) and star (HH34). Note that measurements in DG Tau are dominated by bowshock wings and are an upper limit to the true width of the narrower jet core. Taken from Dougados et al. 2000

- *radio jets:* Their transverse width is < 50 AU on 50 AU scale, consistent with optical sizes (cf. above; Rodriguez, Anglada, Raga 1995). The most stringent upper limit derives from an observation at 7mm of the jet from the Class I/II source HL Tau, at a resolution of $0.04'' = 6$ AU (see Fig. 5 in Eisloeffel et al. 2000); the jet width does appear to decrease markedly between 50 AU and 10 AU of the source. Powerful clues to jet structure below the beam resolution are contained in the variation of emission size and flux density with frequency (see Reynolds 1986). In particular, if the ionization fraction, velocity, and temperature are roughly constant, they can be modelled by a jet width varying with distance as $r \propto d^{\epsilon}$, with $\epsilon \leq 1$, i.e. a reconfined jet (Rodriguez 1995; Anglada 1996), already collimated within 10 AU of the star (Anglada et al. 1998).

- *molecular jets:* The CO jet in HH 211, imaged at a resolution of 400 AU, is well resolved in its intermediate section and its width fluctuates markedly (Gueth & Guilloteau 1999). However, higher resolution observations reveal that the broadest parts correspond to small bows or cavity structures, while a faint central beam remains unresolved, with a width ≤ 250 AU (Chandler & Richer 2001, Gueth 1997). When mapped, bipolar water masers systems are confined inside a beam diameter of only 8-20 AU at a distance of 20-40 AU (Chernin 1995; Claussen et al. 1998; Furuya et al. 1999), comparable to radio and optical jet widths on the same scale in Class II sources. In the HH 1 jet, similar widths are measured in H_2 2.12μm and in [Fe II] within the errors (Reipurth et al. 2000a). Based on current data, there appears to be surprisingly little difference between molecular and atomic jet widths.

2 Kinematics and time variability

2.1 Jet radial velocities and proper motions

- *Molecular jets:* Their kinematics is characterized by a roughly linear increase in radial velocity with distance from the source. In CO or SiO, radial velocity increases from very low values up to 40 km s^{-1} to 150 km s^{-1} over a scale of 1,200-20,000 AU (Guilloteau et al. 1992; Gueth & Guilloteau 1999; Bachiller et al. 2000). Water masers within 100 AU of the source show a much steeper gradient (0.74 km s^{-1}/AU in S106 FIR). The spatial gradient probably does not trace actual acceleration but rather a range of velocities in a bowshock-like structure: individual maser spots in S106 FIR measured over two epochs present a line-of-sight acceleration of only 1-2 km s^{-1}/yr, much smaller than expected from the observed radial velocity gradient (0.74 km s^{-1}/AU) and proper motion (12 AU/yr) (Furuya et al. 1999). Correction of flow speeds for inclination has only been possible in a few cases so far; In water masers, proper motions indicate velocities of 45-65 km s^{-1} at 25-40 AU from the source (Claussen et al. 1998, Furuya et al. 1999). In the HH 111 jet, inclination is known independently from optical radial velocities and proper motions. CO radial velocities of 40 km s^{-1} in the outer molecular bullets then correspond to a space velocity of 240 km s^{-1} (Cernicharo & Reipurth 1996).

- *Optical jets:* The bright jet beam sections generally have broad line profiles, extending from blueshifted radial velocities of 100-400 km/s down to the ambient cloud velocity, as illustrated in Fig. 7 for HH 111 (Reipurth et al. 1997). The lower velocity gas often appears to accelerate away from the source over a scale of 10,000 AU, and to be located toward the jet edges (Solf 1987; Hartigan et al. 1993). Jet radial velocities tend to increase with luminosity of the central star, and 20%-70% variations along the jet are seen in half the cases studied (Mundt 1992). Proper motions of 100-500 km s^{-1} are typically measured for the jet knots (e.g. Hartigan et al. 2001), but values as high as 1000 km s^{-1} are encountered in radio jets driven by sources of 10^4 $L_\odot$ (Marti, Rodriguez, Reipurth 1995; Rodriguez et al. 2001). No evidence for helical motions has been found so far.

- *microjets in Class II sources:* An atlas of long-slit spectra of microjets with typical resolution of 200 AU is presented in Hirth et al. (1997) (see also Solf 1997). Observations at higher spatial resolution of the DG Tau microjet are shown in Figure 7 (right panel) and illustrate typical trends: The maximum [O I]λ6300 radial velocity and line width in the microjet are reached very close to the star ($\leq 1'' = 140$ AU). As low-velocity emission accelerates and fades away, the profile becomes narrower, with peak radial velocities of 100-400 km s^{-1} that stay constant or decrease with distance. In DG Tau, a faint, broad slow flow remains visible out to 600 AU around the fast jet core (Mundt et al. 1987; Lavalley et al. 1997, Lavalley-Fouquet et al. 2000, Bacciotti et al. 2000). [N II]λ6583 peaks at the blue edge of [O I]λ6300 and slightly further from the star, indicating an increase in ionization with flow speed and distance. Radial velocity asymetries between jet and counterjet are sometimes seen (Hirth et al. 1994). In addition to the extended microjet, a compact near rest-velocity [O I]λ6300 component is always detected toward the star, and attributed to the base of a disk wind (cf. Solf 1997 and Section 8). Proper motions of 100-200 km s^{-1} are measured for knots in T Tauri jets (cf. Fig. 5; Eisloeffel & Mundt 1998).

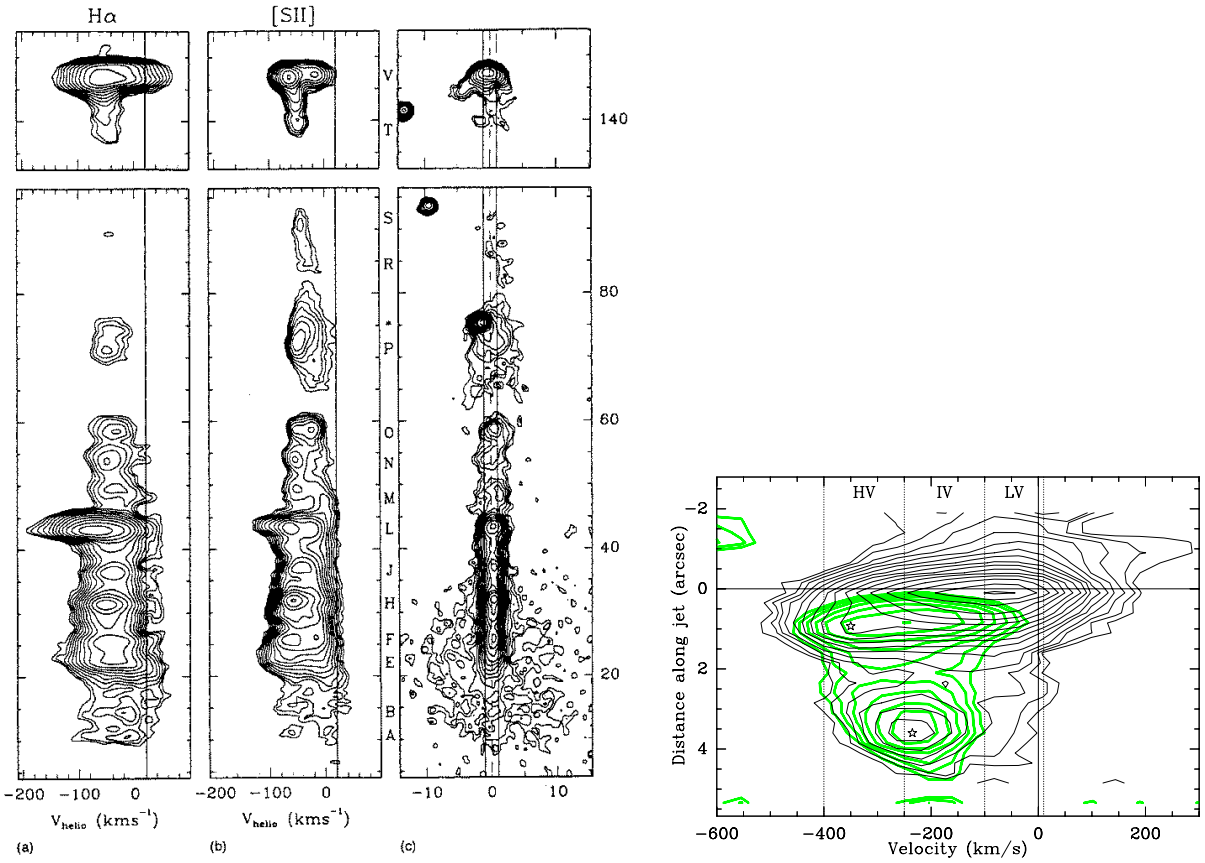

Figure 7: Left panel: Long-slit spectra and image of the HH 111 jet; distance is in arcseconds = 450 AU (from Reipurth et al. 1997); Right panel: Long-slit spectra of the DG Tau microjet in [O I]λ6300 (black) and [N II]λ6583 (grey). 1 arcsec = 140 AU (from Lavalley-Fouquet et al. 2000)

2.2 Herbig-Haro bows and molecular bullets as internal working surfaces

- *Herbig-Haro bows:* The curved morphology of optical HH bows is strongly suggestive of a **bowshock** driven into the ambient medium by the leading working surface of a supersonic jet. Spatial variations in excitation and line shapes, as well as the broad, double-peaked integrated line profile, are indeed well reproduced by bowshock models (see e. g. Reipurth & Raga 1999 and refs. therein). Proper motion studies, e.g that of HH 34 by Eisloeffel and Mundt (1992) shown in Figure 8, globally confirm this interpretation: in the reference frame of the bow apex, proper motion vectors lie tangent to the curved surface, as expected for fluid in a bowshock.

One initially puzzling aspect of the bowshock interpretation is that the shock speed deduced from line ratios in the HH object (40-150 km/s typically) is often much lower than the propagation speed deduced from proper motions and radial velocities. The two facts can only be reconciled if material ahead of the bowshock is already moving at a substantial fraction of the jet speed, i.e. if the bowshock is not the true head of the jet (e.g. Heathcote & Reipurth 1992). This explanation is supported by the discovery of more distant HH objects in many Class I jets and superjets.

If HH bowshocks are not created by the passage of the leading jet head, what is their origin ? The impressive symmetry, both in location and in radial velocity, between major bowshocks on

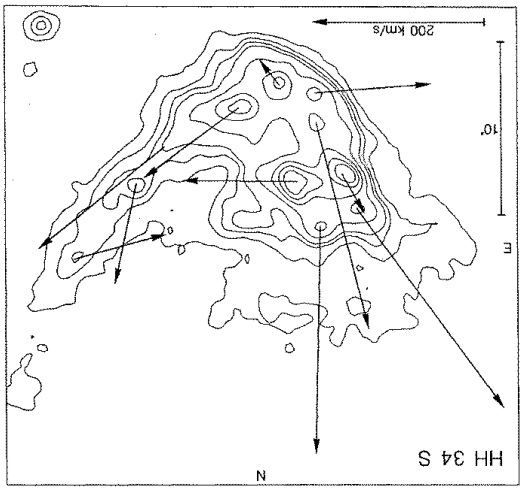

Figure 8: Proper motions of the Herbig-Haro object HH 34 S, in the reference frame of the bow apex, suggestive of fluid sliding along a bowshock surface. Image is rotated in the same way as Fig. 4, with the exciting source towards the bottom. From Eisloeffel & Mundt 1992

the jet and counterjet sides (e.g. in the HH 34 superjet, Devine et al. 1997), rules out external causes and implies that they must be created by an intrinsic jet process (variability and/or instability).

Raga et al. (1990) showed that a two-sided shock (**internal working surface**) will form in the jet beam when the jet is overtaking slower moving ejecta. High-pressure material between the two shocks is ejected sideways and interacts with surrounding slower material, forming a new bowshock structure (Raga & Kaufman 1992; Reipurth & Raga 1999). At large distances, all jet material eventually gathers into a few large bowshocks.

In simple models of sinusoidal time variability of the jet injection velocity, the spacing Δx between internal working surfaces is related to the period of the velocity variability, τ, and the jet mean velocity $\bar{v}$ by $\Delta x = \bar{v}\tau$.The spacing between major bowshocks in superjets, 0.2 pc, and typical jet velocity of 200-400km s^{-1}, would then indicate a variability timescale of order 500-1000 years. This is reminiscent of the duty cycle for FU Ori-type eruptive events, and might be related to orbital interactions within excentric multiple systems (Reipurth 2000).

Another characteristic of successive HH bows is that they often show apparent deceleration away from the central source, by a factor 5-10 in the HH 34 superjet, (Devine et al. 1997). Cabrit & Raga (2000) show analytically that non-extreme jet velocity variability at the source cannot produce a deceleration factor ≥ 2. This favors progressive deceleration of the internal bowshocks as they loose momentum to slower material around the jet beam (see also Gouveia dal Pino 2001). The large scale "S-shape" curvature of some HH superjets suggests precession, which would enhance interaction of the variable jet with its surrounding (Raga & Biro 1993).

-*Molecular bullets:* The well-studied chains of molecular bullets in L 1448 and HH 111 (Bachiller et al. 1990; Cernicharo & Reipurth 1996) share many kinematic similarities with large optical HH bows : (1) High spatial and velocity symmetry between jet and counterjet sides; (2) regular spacing $\simeq$ 0.05-0.1 pc; (3) Apparent deceleration away from the central source beyond 0.1 pc; (4) Comparable radial velocity in CO and optical lines, when both are detected (bowshock V of HH 111). These similarities strongly support the suggestion of Bachiller et al. (1991a) that molecular bullets could represent the precursors of optical HH bowshocks.

2.3 Nature of inner jet knots

Optical jets and microjets: The origin of small scale knots in bright Class I jet beams has been heavily debated. An early suggestion was they were stationary crossing shocks where jets adjusted in pressure with the environment. This was dismissed by measurements of very high proper motions. Kelvin-Helmoltz instabilities at the jet/cloud interface were also invoked, based in particular on some discrepancies between the knot pattern speed and deprojected fluid velocity (see e.g. Eisloeffel & Mundt 1992). However, the very high degree of symmetry between jet and counterjet knots within 0.1 pc of the source observed in the infrared H_2 jet HH 212 challenges this interpretation (Zinnecker et al. 1998). A process intrinsic to the jet must again be at work.

Travelling jet instabilities have been proposed (see Reipurth & Raga 1999 and refs. therein). Another possibility would be, as for larger HH objects, internal working surfaces caused by jet velocity variability. Support for the latter hypothesis includes: (1) intensity decreasing with distance as expected for internal working surfaces (Raga & Kofman 1992); (2) morphology and kinematics of "mini-bowshocks" in well-resolved knots (e.g. Lavalley et al. 1997); (3) Radial velocity variations and appearance of new knots at the source position over a few years (Solf 1997; Marti et al. 1995). The typical knot spacing of 500-1000 AU and jet velocity of 300 km/s suggests a timescale of 10-20 years, though several timescales are probably present (Hester et al. 1998; Raga & Noriega-Crespo 1998). Jet wiggles and one-sided Hα arcs further suggest jet precession over similar timescales (Marti et al. 1993; Reipurth et al. 1997).

Molecular jets: Comparison of the HH 211 CO jet in Figure 2 with the HH 34 jet in Figure 4 shows that the spacing of knots is very similar in both cases. Subarcsecond resolution observations in CO and in SiO reveal curved knots very similar to the "mini-bowshocks" in optical jets (Gueth 1997; Chandler & Richer 2001). Again, a similar origin is strongly suggested.

3 Jet density and excitation conditions

3.1 Molecular jets

- *Method:* A detailed description of infrared and radio molecular lines as physical diagnostics is given by Genzel (1991). Since CO is very stable, masses are usually derived from its column density, adopting a typical abundance ratio $CO/H_2 \simeq 10^{-4}$. The column density is inferred from the line surface brightness, using the optical depth τ and the excitation temperature of the transition T_{ex} estimated from ratios of various transitions, in LTE (see Bachiller & Tafalla 1999). Note that when T_{ex} exceeds the energy of the upper level of the transition ($T_{up} = 11$ K for the CO(2-1) line), emission becomes inversely proportional to T_{ex}, due to the partition function, hence this is an important parameter. For transitions of high critical density, such as high-J CO lines or SiO lines, non-LTE analysis with a Large-Velocity-Gradient (LVG) method may be used to constrain the H_2 density, kinetic temperature, and species column density along the line of sight.

- *Outer molecular bullets:* They contain gas at a range of temperatures: Line ratios involving CO(4-3) and CO(3-2), as well as the inversion transitions of NH_3, give values of $T_{ex} \simeq$ 50-100 K, while earlier estimates using CO(2-1)/(1-0) give 15 K only (Hatchell et al. 1999 and references therein; Nisini et al. 2000). Whenever observed, rovibrational lines of H_2 indicate even higher temperatures $\simeq$ 2000 K but they sample a much smaller column density (Gredel 1994; Buckle

et al. 1999). Individual bullet masses are dominated by the warm component, and range from 10^{-3} $M_\odot$ (HH 111) to 10^{-2} $M_\odot$ (Cep E). For a typical bullet diameter of 5″ at 500 pc, the average density is then $n_{\rm H_2} \simeq 10^4 - 10^5$ cm^{-3}. Analysis of SiO lines in L1448 indicate bullet densities in the range $1 - 7 \times 10^5$ cm^{-3}, decreasing with distance, while the SiO/CO abundance is greatly enhanced by $\geq 10^4$ (e.g. Bachiller et al. 1991a). This, and the elevated temperatures compared to the ambient cloud, indicate the presence of shocks sufficiently powerful to have removed silicon from dust grains (Martin-Pintado, Bachiller, & Fuente 1992).

- *Inner jet beam:* In the HH 211 jet, CO(2-1) probes a total mass of $2.5 \times 10^{-3} (T_{\rm ex}/50\ K)\ M_\odot$. If the whole apparent volume of the jet is filled, the inferred density is of order 10^5 cm^{-3} (Gueth & Guilloteau 1999). The detection of SiO(5-4) suggests even higher densities, comparable to the critical density for exciting that line, $n_c \simeq 10^6$ cm^{-3}. The SiO (5-4)/(1-0) ratio yields $T_{\rm ex} \geq 120 - 180$ K, and the SiO abundance is enhanced by $\simeq 10^6$ (Chandler & Richer 2001). Similar high densities are estimated in the L 1448 molecular jet at 30-3000 AU from the source (Bachiller et al. 1991a; Chernin 1995).

3.2 Optical jets and HH objects

3.2.1 Line excitation mechanism

It is well established that the optical line emission spectrum in HH objects is well reproduced by shock waves with speeds 20-100km s^{-1} and pre-shock densities in the range 10-1000cm^{-3}, although some puzzling discrepancies with basic models still remain (Raga et al. 1996; Hartigan et al. 2000). The line excitation mechanism in optical jet beams has been more debated. Four heating processes have been invoked: (1) radiative shocks, (2) turbulent viscosity in a mixing layer at the edge of the jet, (3) ion-neutral drift in a magnetized wind ("ambipolar diffusion"), and (4) jet compression by travelling instabilities. Recently, it has been possible to discriminate between models (1), (2) and (3) by comparing observed line ratios with detailed theoretical predictions of the optical spectrum (Hartigan et al. 1994; Binette et al. 1999; Garcia et al. 2001a,b). In model (4), the temperature depends very sensitively on the compression angle, precluding a general analysis (Bacciotti et al. 1995). Discriminant line ratio diagrams using [N II]λ6583, [O I]λ6300 and [S II]λ6731,λ6716 are shown in Figure 9**a,b,c,d** (see Lavalley-Fouquet et al. 2000).

In the top diagram, which plots [N II]λ6583/[O I]λ6300 vs [S II]λ6731/[O I]λ6300 (Fig. 9**a,c**), the observed points in microjets and HH objects are found to fall right in the range expected for shock models with preshock densities $10^2 - 10^5$cm^{-3} (grey curves); in contrast, models of mixing-layers and magnetic winds heated by ambipolar diffusion have insufficient [N II]λ6583/[O I]λ6300, due to their low ionization. In the bottom diagram, which plots [S II]λ6716/λ6731 vs. [S II]λ6731/[O I]λ6300 (Figure 9**b,d**), all observed line ratios follow closely the grey "sequence" corresponding to planar shock models. This sequence arises from the almost constant temperature of $\simeq$ 8000 K in the forbidden line emitting region behind shock fronts (Hartigan et al. 1994). In contrast, the hotter models with $T_{\rm e} \geq 10^4$ K (mixing-layers and magnetic winds heated by ambipolar diffusion) are displaced to the left of the observed points. Hence, in jets and microjets studied so far, shocks appear as the dominant line excitation mechanism down to 30 AU of the star.

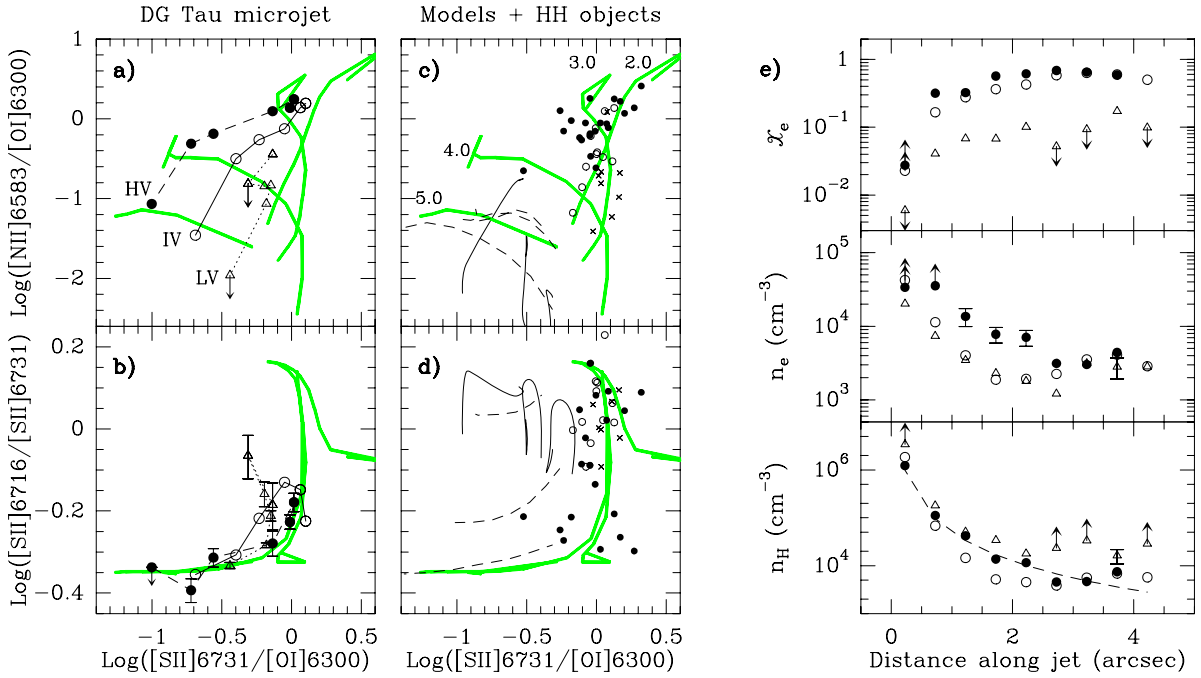

Figure 9: **a,b,c,d:** Comparison of observed line ratios (symbols) in the DG Tau microjet (**a,b**) and in HH objects and jets (**c,d**, Raga et al. 1996), with predictions of various line excitation models: planar shocks (grey curves; Hartigan et al. 1994), mixing layers (dashed curves; Binette et al. 1999), and ambipolar diffusion heated magnetic disk winds (solid curves; Garcia et al. 2001). Shocks best reproduce the observed line ratios. **e:** Ionization fraction x_e, electronic density n_e, and total density $n_H = n_e/x_e$, in the DG Tau microjet as a function of distance (1" = 140 AU), using the procedure of Bacciotti & Eisloeffel (1999). From Lavalley-Fouquet et al. (2000).

3.2.2 Density and ionization from forbidden line ratios

- *Methods:* The [S II]λ6716/λ6731 doublet ratio is a well-known direct diagnostic of the electronic density n_e, almost independent of temperature (Osterbrok 1989). To obtain the total density n_H in the emitting region, which is the critical constraint on ejection models, one then needs to correct for the ionization fraction $x_e = n_e/n_H$. Since shocks appear as the dominant excitation mechanism, the most accurate method consists in comparing various line ratios with shock models (Hartigan et al. 1994). An alternative method introduced by Bacciotti et al. (1995) and improved by Bacciotti & Eisloeffel 1999 (hereafter BE99) infers x_e and T_e from the [N II]λ6583/[O I]λ6300 ratio (mostly sensitive to x_e), the [S II]λ6731/[O I]λ6300 ratio (mostly sensitive to T_e), and the measured n_e. A critical assumption is that N^+/N has reached ionization equilibrium at T_e, while $x_e = H^+/H$ has not necessarily done so. This is only justified for $T_e < 2 \times 10^4$ K (Lavalley 2000). Such an approach also assumes a uniform emission region, and is therefore not exact in regions with strong gradients. In shocks, T_e is overestimated when $V_{shock} \geq 50$ km s^{-1} by up to a factor 2.5 (Lavalley 2000), but x_e is less severely overestimated, by 50% typically for preshock densities $10^3 - 10^4$ cm^{-3} (BE99). Hence this method remains useful for estimating x_e at many positions and velocities.

- *Results:* Values of n_e range from $\geq 4 \times 10^4$ cm^{-3} at the base of T Tauri star microjets down to a few 10-100 cm^{-3} in distant HH objects. Estimates of x_e and n_H as a function of distance have been made with the BE99 method for Class I and II jets (Bacciotti & Eisloeffel 1999,

Bacciotti et al. 1999, Lavalley-Fouquet et al. 2000). All Class II jets (HH 30, Th 28, DG Tau) follow the same pattern, illustrated in Figure 9**e** for DG Tau: Ionization rapidly increases away from the star up to $x_{\rm e}\simeq$ 0.5 at distances of 300-1000 AU while $n_{\rm H}$ drops sharply from a few $10^5 - 10^6$ cm^{-3} at 30 AU to $\simeq 10^3 - 10^4$ cm^{-3} at 600 AU. On larger scales, in Class I jets, $x_{\rm e}$ is much lower and tends to decrease away from the source while $n_{\rm H}$ is roughly constant, with local maxima at the position of major HH knots.

Detailed comparison with shock models has been conducted for a few jets: The Class I jets of Fig. 4 have typical $V_{\rm shock}$ of 30 km s^{-1}, very low ionization fractions of 0.02-0.04, and densities $n_{\rm H}= n_{\rm e}/x_{\rm e}\simeq 7\times10^3 - 4\times10^4$ cm^{-3} on scales of 0.1pc (Hartigan et al. 1994). In the DG Tau microjet, one infers higher shock speeds of 70-100 km s^{-1} at high velocity, and 50-60 km s^{-1} at intermediate velocity (Lavalley-Fouquet et al. 2000). The resulting $x_{\rm e}$ and $n_{\rm H}$ are very similar to those derived with the BE99 method (see Fig. 9**e**). In HH 111 and DG Tau, shock speeds are compatible with observed radial velocity variations along the jet, after correction for inclination. This sets an upper limit on the magnetic field perpendicular to the shock of $\leq$ 1 mG (Hartigan et al. 2001).

4 Estimating mass-loss rates from direct jet observations

A variety of methods have been proposed in the literature to derive the mass-loss rate, $\dot{M}_j$, in young stellar objects. A first class of methods derives $\dot{M}_j$ from direct jet observations. The assumptions and associated uncertainties are described in detail in this section. It should be kept in mind that, whatever the method, the *observable* mass-loss rate could be either an upper limit (if part of the "jet" is tracing entrained ambient material) or a lower limit (if some ejected material is too cool and/or too diffuse to emit).

A second approach for estimating wind dynamics uses its interaction with ambient material, manifested in the form of slow molecular outflows and shock-excited emission lines from the wind/cloud interface. Unlike direct jet observations, these estimates are *integrated over all solid angles and independent of the wind excitation conditions or chemical composition.* This second class of methods will be discussed in Section 6.

4.1 Atomic jet component seen in forbidden lines

4.1.1 Methods based on the jet density and cross-section

These methods, which are free of extinction corrections, determine the mass-loss rate $\dot{M}_j$ from estimates of the mean jet density n_j, velocity V_j, and radius r_j (when spatially resolved):

$$\dot{M}_j = 10^{-7}\left(\frac{n_j}{10^4{\rm cm}^{-3}}\right)\left(\frac{r_j}{150{\rm AU}}\right)^2\left(\frac{V_j}{200{\rm km\,s}^{-1}}\right) M_\odot{\rm yr}^{-1}. \quad (1)$$

Two different assumptions can be used to derive the mean jet density n_j from the measured density $n_{\rm H}= n_{\rm e}/x_{\rm e}$, derived as discussed in Section 3.2.2.

(A.1) Physical conditions are uniform within the observing pixel:

Then, no compression correction is necessary and $n_j= n_{\rm H}$ (Bacciotti & Eisloeffel 1999). This method is probably an *upper limit* to the actual mass-loss rate: If the beam contains a mixture

of high and low density regions, $n_{\rm H}$ will probably be dominated by the high density, high emissivity ones.

(A.2) Emission comes from a shock wave:

Then, n_j can be taken as the preshock density, i.e., $n_j = n_{\rm H} \times C^{-1}$ where C is the compression factor in the shocked layer where the lines are emitted, estimated from comparison of observed line ratios with shock models (Hartigan et al. 1994). Actually, Hartigan et al. recommend to apply $\sqrt{C^{-1}}$ rather than C^{-1} as compression correction: 1D hydrodynamical simulations suggest that it gives a better estimate of the average jet mass flux in the presence of velocity variability; ejected material tends to accumulate in the shocks, diminishing the mass-flux in the freely-flowing segments between shocks.

4.1.2 Methods based on the jet luminosity

Luminosity-based methods have the advantage of being independent of the jet beam radius (which is quite uncertain close to the star), but at the cost of an uncertainty in the extinction correction. The two methods are presented in detail in Appendix A of Hartigan et al. (1995).

(B.1) Physical conditions are uniform within the observing pixel:

The mass-loss rate is simply given by

$$\dot{M}_j = M V_\perp / l_\perp , \tag{2}$$

where M is the jet mass, derived from the (optically thin) forbidden line luminosity, and $V_\perp$ and $l_\perp$ are the projected jet velocity and length in the plane of the sky. For the [S II]6731 line one finds, assuming all sulfur is singly ionized (Equ. A10 of Hartigan et al. 1995)

$$\dot{M}_j = 3 \times 10^{-8} \left(1 + \frac{n_c(6731)}{n_e}\right) \left(\frac{L(6731)}{10^{-4} L_\odot}\right) \left(\frac{V_\perp}{150 \mathrm{km\ s^{-1}}}\right) \left(\frac{l_\perp}{2 \times 10^{15} \mathrm{cm}}\right)^{-1} M_\odot \mathrm{yr}^{-1}, \tag{3}$$

where $n_c(6731) = 1.3 \times 10^4 \mathrm{cm}^{-3}$ is the critical density for collisional deexcitation. Similarly, for the [O I]λ6300 line, $n_c(6300) = 2 \times 10^6 \mathrm{cm}^{-3}$ at a representative temperature of 8200 K, and

$$\dot{M}_j = 2 \times 10^{-10} \left(1 + \frac{n_c(6300)}{n_e}\right) \left(\frac{L(6300)}{10^{-4} L_\odot}\right) \left(\frac{1}{1 - x_e}\right) \left(\frac{V_\perp}{150 \mathrm{km\ s^{-1}}}\right) \left(\frac{l_\perp}{2 \times 10^{15} \mathrm{cm}}\right)^{-1} M_\odot \mathrm{yr}^{-1}. \tag{4}$$

The above expression is derived from equation A8 of Hartigan et al. (1995), with an additional correction factor for oxygen ionization (assuming that, through charge exchange, $O^+/O = H^+/H$).

(B.2) Emission traces cooling in a shock wave:

Hollenbach & McKee (1989) find a quasi-proportionality between the [O I]63μm line luminosity and the mass-flux through a shock, $\dot{M}_{\rm shock}$. The same roughly applies to the [O I]λ6300 line (Hartigan et al. 1995). This behavior is understood with the following simple argument: Let us assume that the [O I]λ6300 line represents a fixed fraction $1/f$ of the shock cooling in the temperature range T_2 to T_1. Then, if $N(T_2, T_1)$ denotes the number of atoms of postshock gas in this same range,

$$f L(\mathrm{line}) = L_{cool} \simeq \frac{3}{2} k (T_2 - T_1) \times \frac{N(T_2, T_1)}{t_{cool}(T_2, T_1)} \simeq \frac{3}{2} k (T_2 - T_1) \frac{\dot{M}_{shock}}{\mu m_H}. \tag{5}$$

A proportionality between L(line) and $\dot{M}_{\rm shock}$ is thus predicted as long as f does not vary greatly with shock conditions (which is justified at preshock densities $\geq 10^5$ cm^{-3}). To derive $\dot{M}_j$ from $\dot{M}_{\rm shock}$, an assumption must be made about the shock geometry. For a moving shock intercepting the whole jet beam, and perpendicular to the jet flow, $\dot{M}_j = (V_j/V_{\rm shock})\ \dot{M}_{\rm shock}$. Quantitatively, Hartigan et al. find:

$$\dot{M}_j = 5 \times 10^{-7} \left(\frac{L(6300)}{10^{-4} L_\odot}\right) \left(\frac{\cos\mu}{N_{shock}}\right) \left(\frac{V_j/300{\rm km\ s^{-1}}}{V_{shock}/40{\rm km\ s^{-1}}}\right) M_\odot {\rm yr}^{-1} \quad (6)$$

The above expression is derived from Equ. A17 of Hartigan et al. (1995), with an additional correction factor $\cos\mu/N_{shock}$, where N_{shock} is the number of shocks within the beam, and μ is the angle of the shock from the perpendicular to the jet flow. In the particular case of a stationary oblique shock, $V_{\rm shock} = \cos\mu V_j$ and $\dot{M}_j = \dot{M}_{\rm shock}$.

4.1.3 Comparison of the 4 methods: Class I jets and the DG Tau microjet

Since the above 4 methods all use the same tracer: forbidden lines, it is instructive to compare the resulting $\dot{M}_j$, as an indicator of uncertainties. Table 1 presents such a comparison for the three bright Class I jets of Figure 4: HH 34, HH 47, and HH 111. The table lists planar shock model parameters $<x_{\rm e}>$, $\sqrt{C}$, and $V_{\rm shock}$ determined from 5 different line ratios by Hartigan et al. (1994), and their published values of $\dot{M}_j$ using methods *(A.2)* and *(B.1)*. In addition, the table also lists $\dot{M}_j$ for method *(A.1)*, using the values of $x_{\rm e}$(BE) derived by Bacciotti & Eisloeffel (1999) with their procedure, and $\dot{M}_j$ for method *(B.2)*, assuming $\cos\mu/N_{\rm shock} = 1$.

As $x_{\rm e}$ and $n_{\rm e}$ actually vary along the jet (e.g. Bacciotti & Eisloeffel 1999) and with radial velocity inside the line profile (e.g. Lavalley-Fouquet et al. 2000) it is also instructive to perform a comparison as a function of distance and flow speed . This is done in Figure 10 for the microjet from the Class II source DG Tau, using 80 AU pixels (Lavalley 2000).

Table 1: Comparison of 4 mass-loss rate derivations from optical lines in Class I jets

Jet	n_e	$x_e(BE)$	$<x_{\rm e}>$	$\sqrt{C}$	$V_j/V_{\rm shock}$	Cross-section		[O I] luminosity	
	(cm^{-3})				(km s^{-1})	uniform	shock	uniform	shock
						(A.1)	*(A.2)*	*(B.1)*	*(B.2)*
HH 34	650	0.027	0.016	4.0	220/28	4.0 10^{-7}	1.7 10^{-7}	1.5 10^{-7}	4.5 10^{-6}
HH 47	250	0.070	0.036	4.9	350/34	9.8 10^{-7}	3.9 10^{-7}	4.2 10^{-7}	4.6 10^{-5}
HH 111	900	0.064	0.027	4.7	320/32	3.6 10^{-7}	1.8 10^{-7}	5.8 10^{-7}	2.9 10^{-5}

Among the two methods assuming uniform emission, the cross-section based estimate *(A.1)* is always higher than that expected from the observed [O I]λ6300 luminosity *(B.1)*, for both Class I jets and the DG Tau microjet. It suggests that the local $n_{\rm H}$ is higher than the average density in the jet volume. A filling factor < 1 is similarly derived by Bacciotti et al. (1999) for the HH 30 jet. Hence *(A.1)* tends to give an upper limit to the mass-loss rate.

Among the two methods assuming shocks, *(B.2)* derived from the total luminosity is generally higher than *(A.2)*. The difference amounts to 10-100 in Class I jets, where line luminosity was integrated over a section of $10^3 - 10^4$ AU along the jet (2"-20" at 500pc; Hartigan et al. 1994). It would suggest that $N_{\rm shock}/\cos\mu \simeq 1$ per 100 AU of jet length. The difference is less severe in DG Tau, a factor of 1-4 typically; the smaller pixel of 80 AU includes less shocks. Overall, *(B.2)* does not appear reliable unless small pixels ≤ 100 AU are used.

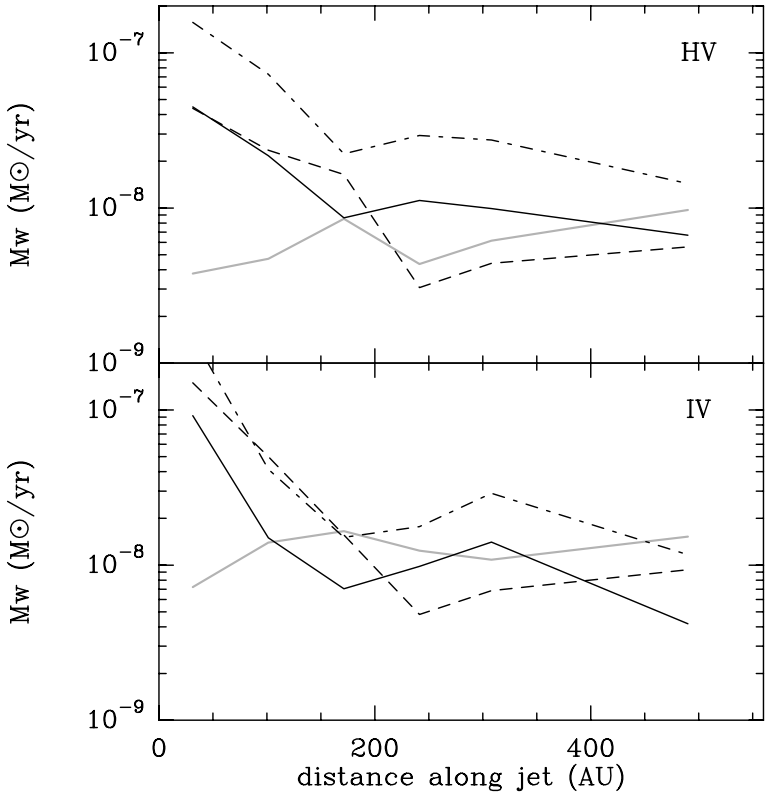

Figure 10: Mass-loss rate in the DG Tau microjet as a function of distance for two different velocity ranges: Top panel: high-velocity [-400,-250]km s^{-1}, bottom panel: intermediate velocity [-250,-100]km s^{-1}. Curve styles refer to the four different methods: Using the jet cross-section, and assuming uniform emission (A.1, dash-dot) or a shock (A.2, solid line); [O I]λ6300 luminosity, assuming uniform emission (B.1, grey line) or a single shock (B.2, dashed, with $\mu/N_{\rm shock}$ = 1). Adapted from Lavalley (2000).

The most reliable methods thus appear to be *(A.2)* and *(B.1)*. Interestingly, they give very similar results within a factor 3 in Class I jets, as well as in the DG Tau microjet beyond 100 AU of the source. Closer to DG Tau, however, the two methods become discrepant, with $\dot{M}_j$*(A.2)* increasing by almost a factor 10 while $\dot{M}_j$*(B.1)* decreases. The latter could be due to extinction, and the former to an overestimated jet radius (close to the resolution limit). Extinction-correction of *(B.1)* using the stellar A_v (3.5 mag towards DG Tau, Hartigan et al. 1995) will give the correct value if the increase in $\dot{M}_j$*(A.2)* is real, and an upper limit otherwise, if the larger scale value is more representative.

4.2 Mass flux in molecular jets and bullets

- *molecular jets:* The mass-flux can be calculated from method *(B.1)*: $\dot{M}_j = MV_\perp/l_\perp$, using the jet mass and size derived from CO or SiO jet maps, and a characteristic expansion speed. In HH 211 ($\simeq$ 10 $L_\odot$; Gueth & Guilloteau 1999) and IRAS 20126+4104 (10^4 $L_\odot$; Cesaroni et al. 1999) one finds

$$\dot{M}_j = 4\times10^{-6}\times(V_\perp/100{\rm kms}^{-1})M_\odot{\rm yr}^{-1} \quad (7)$$

$$\dot{M}_j = 2\times10^{-3}[2\,10^{-9}]/[{\rm SiO/H_2}]\times(V_\perp/100{\rm kms}^{-1})M_\odot{\rm yr}^{-1} \quad (8)$$

- *molecular bullets:* Hatchell et al. (1999) argue convincingly that, at least in the case of

HH 111, molecular bullets are too massive to be made of entrained ambient gas. If they trace jet material, shocked and compressed into discrete internal working surfaces, the spacing Δx between bullets may be used to derive an average jet mass-loss rate. With parameters typical of HH 111:

$$< \dot{M}_j >= 4 \times 10^{-6} \left(\frac{M_{\rm bullet}/10^{-3} M_\odot}{\Delta x/0.1{\rm pc}} \right) \left(V_\perp/200{\rm kms}^{-1} \right) M_\odot yr^{-1}. \quad (9)$$

The largest uncertainty comes from the assumed $V_\perp$, the possible contribution of entrained material, and the assumed $T_{\rm ex}$ (and SiO abundance in IRAS 20126+4104).

4.3 Radio jet component

The mass-loss rate in a jet of opening angle $\theta_0 \leq 0.5$ (in radians) and uniform ionization fraction $x_{\rm e}$ is related to the free-free continuum flux S_ν and the spectral index α by (Reynolds 1986):

$$\dot{M}_{-6} = \frac{0.26}{x_e} \left(\frac{V_j}{200\,{\rm kms}^{-1}} \right) \left(\frac{S_\nu\, \theta_0\, D^2}{{\rm mJy\,kpc}^2} \left(\frac{\nu}{5{\rm GHz}} \right)^{-\alpha} \right)^{3/4} \left(\frac{\nu_m}{10\,{\rm GHz}} \right)^{3(\alpha-0.6)/4} \left(\frac{F \sin i^{1/3}}{1.5} \right)^{-3/4} \quad (10)$$

where $\dot{M}_{-6}$ is in units of $10^{-6}\ M_\odot {\rm yr}^{-1}$, i is the jet inclination to the line of sight, ν_m is the turnover frequency above which emission becomes optically thin, and $F = 2.1/[(\alpha + 0.1)(1 + \epsilon + q_T)]$ contains the power-law variation of jet width (ϵ) and temperature (q_T) with distance. The main uncertainties come from the appropriate V_j, $x_{\rm e}$, and θ_0, which are difficult to assess since radio jets are detected on much smaller scales (< 50 AU) than optical jets and are not resolved transversally.

If ionization is provided by UV photons emitted in a wind shock, the cm free-free opacity is roughly proportional to $n_j\ {V_{\rm shock}}^{1.68}$ and the relationship between cm radio flux and mass-loss rate can be written (Curiel et al. 1990; Anglada 1996):

$$\dot{M}_{-6} = \frac{1.6}{f_s} \left(\frac{V_j}{V_{\rm shock}} \right)^{1.68} \left(\frac{V_j}{200\,{\rm kms}^{-1}} \right)^{-0.68} \left(\frac{S_\nu\, D^2}{{\rm mJy\,kpc}^2} \right) \left(\frac{\nu}{5{\rm GHz}} \right)^{0.1} \left(\frac{\tau_\nu}{1 - \exp -\tau_\nu} \right) \left(\frac{T}{10^4} \right)^{-0.45}, \quad (11)$$

where $f_s \leq 1$ denotes the fraction of the total wind solid angle that is shocked and τ_ν is the optical depth, estimated from the radio spectral index. Compared to the previous formulation, the main uncertainties are now in f_s, and $V_j/V_{\rm shock}$, and the overall scaling of $\dot{M}_j$ is 10 times larger.

5 Estimating wind dynamics from its interaction with ambient gas

5.1 Cold swept-up gas in molecular outflows

The momentum-flux and mechanical luminosity in the flow are calculated from the total flow mass $\rm M_{CO}$, length $\rm R_{CO}$, and characteristic speed $\rm V_{CO}$, derived from low excitation CO lines, as:

$$F_{\rm CO} = M_{\rm CO} V_{\rm CO}^2 / R_{\rm CO}, \quad L_{\rm CO} = (1/2) M_{\rm CO} V_{\rm CO}^3 / R_{\rm CO}. \quad (12)$$

Uncertainties caused by optical depth, velocity gradients, and inclination effects, are discussed in detail in Cabrit & Bertout (1990) and reach up to a factor 10. Hidden momentum in dissociated hydrogen is discussed by Downes & Ray (1999).

The above parameters can be related to the wind momentum rate, $F_j = \dot{M}_j V_j$, and mechanical luminosity $L_j = (1/2)\dot{M}_j V_j^2$, through a model of the wind/cloud interaction. The simplest case is a highly radiative, momentum conserving, planar "two-shock structure" perpendicular to the jet (see e.g. Hollenbach 1997). The propagation speed V_{CO} of the molecular flow is fixed by ram pressure equilibrium between shocked ambient gas and shocked jet gas:

$$\rho_a V_{CO}^2 = \rho_j (V_j - V_{CO})^2, \tag{13}$$

where ρ_a and ρ_j are the ambient and jet density (assumed here constant for simplicity). Mutliplying on either side by the shock area A_s and noting that the swept-up molecular mass is $M_{CO} = A_s \rho_a R_{CO}$, one finds

$$F_{CO} = F_j (1 - V_{CO}/V_j)^2 = \eta F_j \tag{14}$$

$$L_{CO} = L_j (V_{CO}/V_j)(1 - V_{CO}/V_j)^2 = \varepsilon_a L_j. \tag{15}$$

The momentum and energy transfer efficiencies η and ε_a are plotted in Figure 11 as a function of V_{CO}/V_j. Note that ε_a is always $\leq 1/7$. The above formulae are not changed if the wind and ambient density have the same variation with distance (e.g. $1/r^2$). In more general density distributions, or if the wind shock is not radiative, extra numerical factors appear in η and ε_a (Dyson 1984).

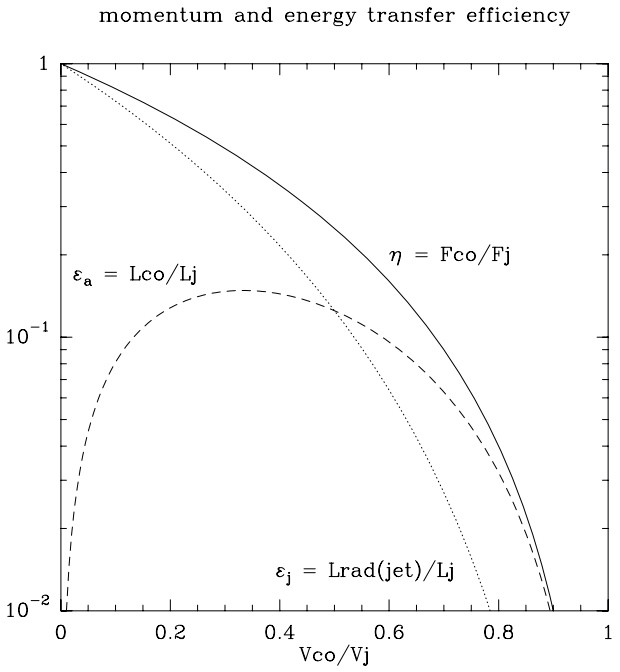

Figure 11: Momentum and energy transfer efficiencies in a planar shock between the jet, of velocity V_j, and the ambient gas, moving with velocity V_{CO}, plotted as a function of V_{CO}/V_j.

5.2 Ambient shock luminosity

One may also use the above simplified model to calculate the luminosity radiated in the ambient shock (where the flow is accelerated) and in the jet shock (where the jet strikes the flow) as:

$$L_{\rm rad}({\rm ambient\,shock}) = (1/2)\rho_a A_s V_{\rm CO}^3 = L_{\rm CO} = \varepsilon_a L_j, \quad (16)$$

$$L_{\rm rad}({\rm jet\,shock}) = (1/2)\rho_j A_s (V_j - V_{\rm CO})^3 = L_{\rm CO}(V_j/V_{\rm CO} - 1) = \varepsilon_j L_j. \quad (17)$$

Figure 11 plots ε_a and ε_j as a function of $V_{\rm CO}/V_j$.

Given the slow propagation speeds in outflows of $V_{\rm CO} \simeq$ 10-40 km s^{-1}, compared to typical jet speeds of 200 km s^{-1}, the jet shock should be a fast, dissociative jump-type (J) shock and emit mostly in UV and in atomic/ionic lines, in particular the [O I]63μm line (cf. Sect. 6.3 below). In constrast, for the typical magnetic field strengths in dark clouds, one expects the ambient shock to be a magnetically-cushioned "continuous" (C) shock, perhaps with a weak J-shock component if stationary state has not yet been reached (see Hollenbach 1997; Pineau des Forêts et al. 1997 and refs therein; Le Bourlot et al. 2001).

The ISO satellite has allowed for the first time to detect important coolants expected in such non-dissociative molecular C-shocks, namely H_2O lines, high-J rotational lines of CO, and pure rotational lines of H_2, which trace warm gas at 300-1000 K (see e.g. Liseau et al. 1996; Nisini et al. 2000). Hence it is now becoming possible to estimate $L_{\rm rad}$ for the ambient shock as an independent measure of $L_{\rm CO}$. Shock models must be used to correct for unobserved lines. Uncertainties are typically a factor 3-5 but will decrease as more of the spectrum becomes accessible, e.g. with the Herschel satellite.

5.3 [O I]63μm luminosity of the wind shock

If the wind shock is indeed a dissociative J-type shock, the [O I]63μm line is expected to be a major coolant for gas below 5000 K. Method *(B.2)* can then be applied, following the scaling in Hollenbach & McKee (1989), valid for $n_0 \leq 10^5 {\rm cm}^{-3}$ and $V_{\rm shock} \leq 10^7/n_0$ km s^{-1}/cm^{-3}:

$$\dot{M}_j = 10^{-6} \left(\frac{L(63\mu{\rm m})}{10^{-2} L_\odot}\right) \left(\frac{\cos\mu}{N_{shock}}\right) \left(\frac{V_j}{V_{shock}}\right) M_\odot {\rm yr}^{-1}. \quad (18)$$

Current beam sizes at this wavelength $\simeq 60''$ do not resolve the emitting regions. However, in sources that drive a slow molecular outflow, it seems reasonable to assume that the [O I]63μm line luminosity integrated over the whole system is dominated by the quasi-stationary wind-shock, where the wind strikes the slow shell of swept-up ambient gas, i.e. $\cos\mu V_j/(V_{\rm shock} N_{\rm shock}) = 1$.

The largest uncertainty comes from the unknown contribution of other regions to the [O I]63μm line (internal jet shocks, shocked ambient gas, infalling envelope, photo-dissociation regions; see Ceccarelli et al. 1997). Measurements of [O I]63μm and resulting $\dot{M}_j$ are presented in Cohen et al. (1988), Liseau et al. (1997) and Ceccarelli et al. (1997). They range from $2 \times 10^{-6} M_\odot {\rm yr}^{-1}$ in sources of $10 L_\odot$, to $10^{-4} M_\odot {\rm yr}^{-1}$ in a source of $10^4 L_\odot$.

6 Accretion-ejection correlations

6.1 Class II and Class I optical jets

Cohen et al. (1989), Cabrit et al. (1990), and Corcoran and Ray (1998b) reported a correlation between the [O I]λ6300 luminosity and the infrared excess luminosity from the disk in T Tauri stars and their higher mass analogs, the Herbig Ae/Be stars, suggesting that the ejection process in Class II sources is powered by disk accretion. The correlation in TTS was quantified by Hartigan et al. (1995), who used the ratio of excess continuum to stellar continuum at 5500 Å ("veiling") and stellar parameters to calculate the accretion rate $\dot{M}_{\rm acc}$; and method *(B.1)* (Equation 4 above), corrected for extinction by the stellar A_v, to calculate $\dot{M}_j$.

Figure 12 plots the resulting relationship between $\dot{M}_{\rm acc}$ and $\dot{M}_j$. The scatter in this plot results not only from uncertainties in jet excitation conditions, but also from the much shorter variability timescales of the veiling ($\leq$ a day) compared to forbidden lines (crossing time of a few yrs). The average ratio $\dot{M}_j/\dot{M}_{\rm acc}$ is of order 0.01. Since then, Gullbring et al. (1998) have revised $\dot{M}_{\rm acc}$ downward by a factor 10 in some stars (see open symbols in Figure 12), suggesting a higher $\dot{M}_j/\dot{M}_{\rm acc}\simeq$ 0.1. This is an upper limit, as extinction corrections on $\dot{M}_j$ could be too high (cf. Section 4.1.3). The ratio should be doubled to take into account the occulted redshifted jet.

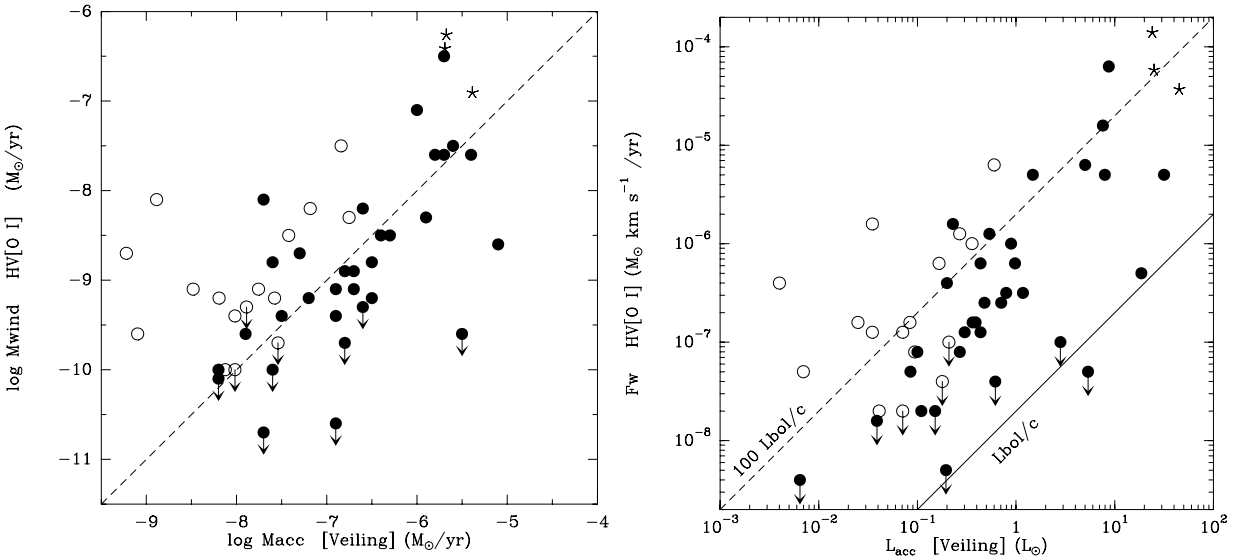

Figure 12: Correlation of the mass-loss rate (left) and momentum rate (right) in the [O I]λ6300 emitting jet with the accretion rate (left) or accretion luminosity (right) for T Tauri stars, from Hartigan et al. (1995; filled circles). Revised accretion rates from Gullbring et al. (1998) are shown as open circles; Class I optical jets from Hartigan, Morse, and Raymond (1994) as star symbols. The dashed line illustrates an ejection/accretion ratio $\dot{M}_j/\dot{M}_{\rm acc}$ of 0.01 (left panel), and a ratio $F_j/({\rm L_{acc}/c})$ of 100 (right panel; cf. Class I sources with molecular outflows in Fig. 14).

In the right panel of Figure 12, the wind momentum supply rate $F_j = \dot{M}_j V_j$ assuming $V_j \simeq$ 200 km s^{-1} is plotted as a function of $L_{\rm acc} = GM_\star \dot{M}_{acc}/R_\star$, where $M_\star$ and $R_\star$ are the stellar mass and radius. For T Tauri stars, one finds $F_j \simeq$ 10-100 $L_{\rm acc}$/c, implying that radiation pressure from the accretion shock or disk is insufficient to drive the jets.

For comparison, the 3 Class I optical jets studied by Hartigan, Morse, Raymond (1994) are also

shown in Figure 12. For consistency we plot values of $\dot{M}_j$ derived with the same method *(B.1)* as for T Tauri stars (cf. Table 1). $\dot{M}_{\rm acc}$ cannot be estimated directly in such embedded sources: Radiation from the star, the accretion disk, and the disk/star boundary layer or accretion shock, is absorbed by the cool dusty envelope and reradiated in the infrared, preventing measurements of optical veiling. The source bolometric luminosity is then $L_{\rm bol}= L_\star + L_{\rm acc}$. An upper limit to $\dot{M}_{\rm acc}$ can be derived assuming typical T Tauri stellar parameters (appropriate at the Class I stage) and $L_{\rm bol}= L_{\rm acc}$ (instead of $L_{\rm bol}= 0.5 L_{\rm acc}$, as in Hartigan et al. 1994):

$$\dot{M}_{acc} = 1.2 \times 10^{-7} \left(\frac{R_\star}{3R_\odot}\right) \left(\frac{M_\star}{0.8M_\odot}\right)^{-1} \left(\frac{L_{acc}}{L_{bol}}\right) \left(\frac{L_{bol}}{L_\odot}\right) M_\odot {\rm yr}^{-1}. \quad (19)$$

Class I jets fall on the upper envelope of the correlation found for TTS jets, with $\dot{M}_j/\dot{M}_{\rm acc} \simeq 0.1$ and $F_j \simeq 100\ L_{\rm acc}/c$. Given the scatter, there is no clear difference in ejection-accretion ratio between the Class I and Class II optical jets. Finally, since the jet speed V_j is probably larger than the escape speed at the stellar surface, the ratio $(\dot{M}_j/\dot{M}_{\rm acc})$ also sets a lower limit to the ratio of the wind mechanical luminosity to the accretion luminosity: $L_j/L_{\rm acc} \geq$ 0.01-0.1

6.2 Molecular outflow sources

6.2.1 $L_{\rm bol}$ as tracer of accretion luminosity in Class 0 sources

The large body of data available on molecular outflows reveals that their momentum flux and mechanical luminosity $F_{\rm CO}$ and $L_{\rm CO}$ are correlated with $L_{\rm bol}$ over a range of 5 orders of magnitude (e.g. Lada 1985; Richer et al. 2000, and references therein). Plots using the sample in Richer et al. (2000) are shown in Figure 13. The sample involves mostly outflows from Class 0 sources: they are well collimated and the exciting source is unambiguously identified. In these very young sources, the central object has not yet reached its final stellar mass and $L_{\rm acc}$ is expected to dominate over $L_\star$, so that $L_{\rm bol}$ should give a rough measure of the accretion level. The following constraints can be set on the ejection mechanism from these correlations:

Momentum supply rate: The correlation with $L_{\rm bol}$ suggests that mass-loss is ultimately driven by accretion power. At luminosities below a few $10^4\ L_\odot$, $F_{\rm CO}$ is 100-1000 times greater than $L_{\rm bol}/c$. If momentum is conserved in the flow acceleration (radiative shocks), then $F_j \geq F_{\rm CO} \gg L_{\rm bol}/c$ and radiatively-driven winds appear ruled out. Thermal and/or magnetic acceleration must be at work. In the highest luminosity sources, $F_{\rm CO}$ is only 10 times $L_{\rm bol}/c$, and radiation pressure might also play a role.

Mechanical luminosity: The ratio $L_{\rm CO}/L_{\rm bol}$ varies from 0.1 in low luminosity sources to 0.01 in high luminosity sources. If momentum is conserved, then $L_j \simeq L_{\rm CO}/\varepsilon_a \geq 7 L_{\rm CO}$. The inferred ratio $L_j/L_{\rm bol}$ is then close to 100% in low luminosity objects, suggesting that *the ejection mechanism extracts a large fraction of the accretion power.* In high luminosity objects, the constraint is $L_j/L_{\rm bol} \geq 10\%$.

Comparison with mass loss estimates in Class 0 sources from shock tracers: Integrated wind mass-loss rates deduced from the [O I]63μm line appear correlated with $L_{\rm bol}$ as (Liseau et al. 1997):

$$\dot{M}_j(63\mu{\rm m}) \simeq 4 \times 10^{-7} (L_{\rm bol}/L_\odot)^{0.6} M_\odot {\rm yr}^{-1}. \quad (20)$$

Assuming $\eta V_j \simeq 150$ km s^{-1}, the momentum transferred to the molecular outflow would follow the relation with $L_{\rm bol}$ shown as a dashed line in Figure 13, which agrees very well with the observed trend for $F_{\rm CO}$ over the whole range of luminosities: In a statistical sense, the [O I]63μm

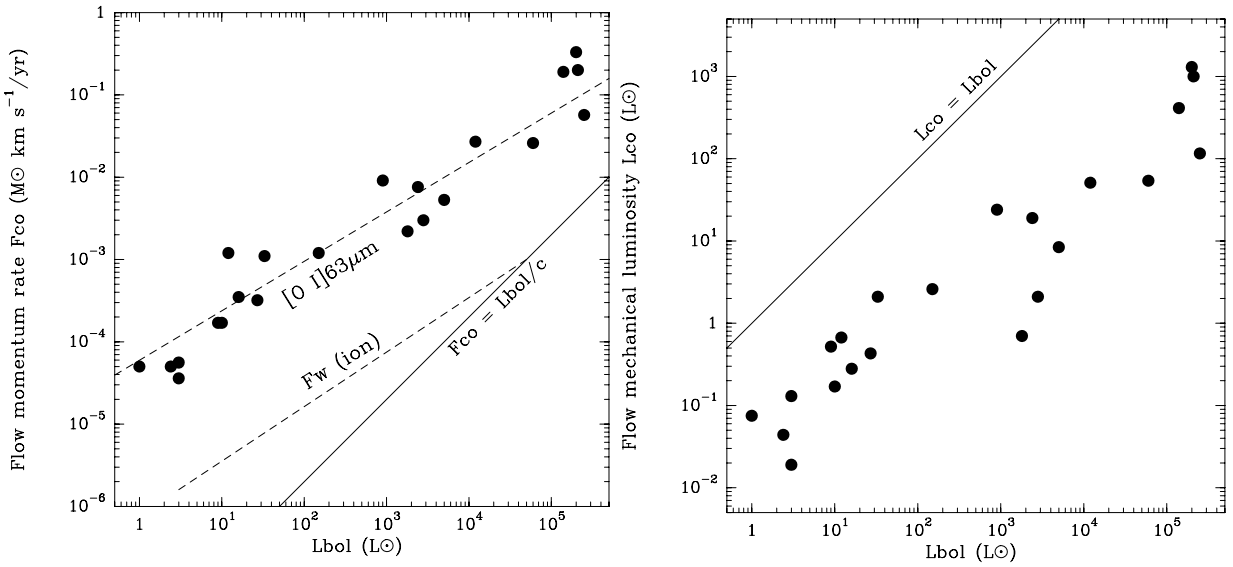

Figure 13: **Left panel:** Correlation of the momentum rate in the swept-up molecular flow, F_{CO} with the source bolometric luminosity L_{bol}. The top dashed line shows the wind momentum rate $\dot{M}_j V_j$ using V_j= 150 km s^{-1} and the $\dot{M}_j$-L_{bol} relation from the [O I]63μm line (Liseau et al. 1997). The bottom dashed line shows the momentum rate in the ionized jet (Panagia 1991). **Right panel:** Correlation of the mechanical luminosity in the swept-up molecular flow, L_{CO} with L_{bol}.

intensity is consistent with Class 0 molecular outflows being momentum-driven by radiative, moderate velocity J-type wind-shocks.

The integrated luminosity of the ambient shock, L_{rad}(ambient-shock), measured from infrared lines of H_2, CO, and H_2O detected with the ISO satellite, is also consistent with this scenario: The total radiated luminosity L_{rad} ranges from 0.1-1$L_\odot$ in sources of 1-10$L_\odot$, to $L_{rad} \simeq 60 L_\odot$ in the Cep A flow, driven by a 10^4 $L_\odot$ infrared source/cluster (Cabrit et al. 1999; Nisini et al. 2000; Froebrich et al. 2002): in all cases, L_{rad} is close to L_{CO}, in agreement with equation 16, i.e. with the hypothesis of a radiative ambient shock.

Can jets drive molecular outflows in Class 0 sources? It has been found that, whenever detected, high-velocity molecular jets/bullets in Class 0 sources have sufficient momentum to drive the associated slow molecular outflows (see e.g. Bachiller et al. 1991b). Furthermore, their typical mass-flux rate, derived in Section 5.2, agrees well with that expected from the $\dot{M}_j$(63μm)-L_{bol} correlation (equation 20 above). Hence, neutral, collimated jets in Class 0 sources are dynamically able to drive the associated molecular outflows, as well as to reproduce the observed level of [O I]63μm line emission.

These jets must be mostly neutral: The momentum supply rate in the ionized component, F_w(ion), inferred from free-free emission assuming a constant velocity (Equation 10) is correlated with L_{bol} with the same slope as F_{CO}, but is shifted down by a factor 10-100 (Panagia 1991; see Figure 13). The radio jet would have enough momentum if its ionization fraction x_e is only 0.01-0.1, as measured in T Tauri microjets 50 AU from the source. Alternatively, radio emission could come from a shock-ionized region intercepting a fraction f_s of the jet, with $f_s (V_j / V_{shock})^{-1.68} \simeq 0.1$ (see Equation 11 and Anglada et al. 1992; Anglada 1996; Cabrit & Bertout 1992).

6.2.2 Envelope mass as tracer of $\dot{M}_{\rm acc}$

A sensitive, uniform survey for weaker molecular outflows around Class I sources of low-luminosity $< 100\ L_\odot$ was made by Bontemps et al. (1996). They found that these flows have $F_{CO} \simeq 100\ L_{bol}/c$ only, whereas molecular outflows from Class 0 sources of similar luminosity have a larger $F_{CO} \geq 1000\ L_{bol}/c$ (Figure 14, left). In contrast, both Class 0 and Class I flows follow a single correlation between F_{CO} and the circumstellar envelope mass M_{env} derived from thermal dust emission (Figure 14, right):

$$F_{\rm CO} \simeq 10^{-4} M_{\rm env} \times {\rm km\ s^{-1} yr^{-1}} \tag{21}$$

Since M_{env} is expected to decrease as the source accretes matter, this correlation suggests

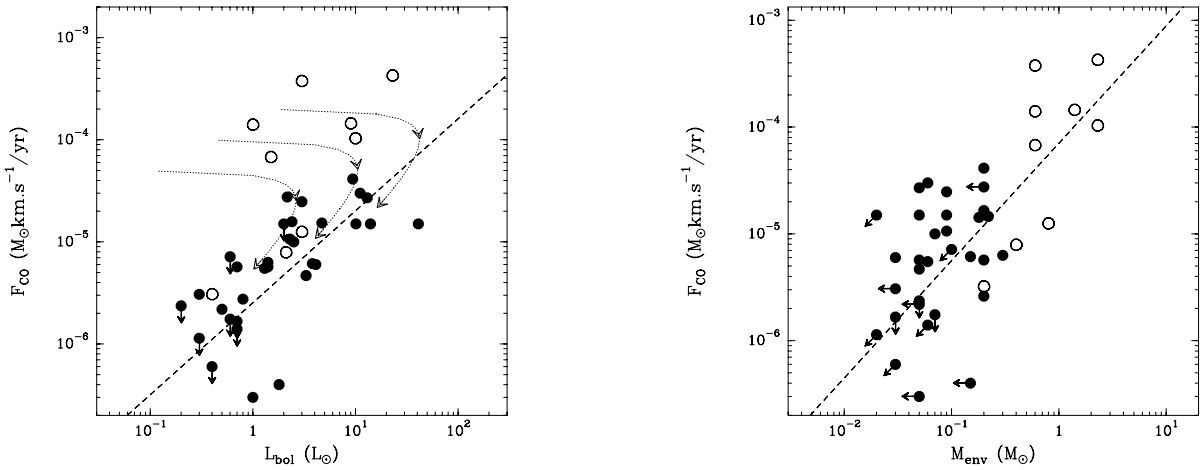

Figure 14: **Left panel:** Correlation of the momentum supply rate in the swept-up molecular flow, F_{CO}, with the source bolometric luminosity L_{bol}. Class 0 sources are shown as open circles and Class I are shown as filled circles. The dashed line corresponds to $F_{CO} \simeq 100\ L_{bol}/c$. Dotted curves with arrows show possible time sequences for $\dot{M}_{\rm acc} = M_{env}/(10^5$ yrs) with initial envelope masses of 0.3,0.6,1.2 $M_\odot$, and a ratio $(\dot{M}_j/\dot{M}_{\rm acc})$ given by equ. 22. **Right panel:** Correlation of F_{CO} with the envelope mass M_{env}, suggesting that both are tightly correlated with $\dot{M}_{\rm acc}$ and decrease in parallel over time. From Bontemps et al. (1996).

a progressive decay of outflow force over time, possibly reflecting a concurrent decrease in accretion rate over time (see also André 1997). Assuming for simplicity that $\dot{M}_{\rm acc} \simeq M_{env}(t)/\tau$, and writing momentum conservation between the jet and flow as $F_{CO} = \eta \times \dot{M}_j V_j$ where $\eta \leq 1$ was defined in Equ.(15), one infers a constraint on the ejection/accretion ratio in low-luminosity outflow sources:

$$\dot{M}_j/\dot{M}_{\rm acc} = 0.07 \left(\frac{\tau/10^5 {\rm yr}}{\eta V_j/150 {\rm kms}^{-1}} \right). \tag{22}$$

A dynamically consistent model of time-dependent infall in protostellar envelopes suggests a slightly lower value of $\eta\ V_j(\dot{M}_j/\dot{M}_{\rm acc}) \simeq 4$ km s^{-1} (Henriksen, André, Bontemps 1997). The temporal evolution in the F_{CO}-L_{bol} plot of an accreting outflow source for a simple model with $\dot{M}_{\rm acc} \simeq M_{env}(t)/(10^5$ yrs) is shown as dotted curves in Figure 14(left panel). It readily reproduces the displacement between Class 0 and Class I sources: For a given L_{acc}, Class 0 sources, being 10 times younger than Class I sources, have 10 times smaller $M_\star$ and 10 times higher $\dot{M}_{\rm acc}$ and F_{CO}. This demonstrates that L_{bol} is not a good tracer of accretion rate when objects of widely different evolutionary stages are compared, and that M_{env} is a better tracer (although one must still take into account luminosity scalings; see Bontemps et al. 1996; André 1997).

Can jets drive molecular outflows in Class I sources? Hartigan et al. (1994) and Bacciotti & Eisloeffel (1999) find that the momentum flux in various optical jets, once corrected for incomplete ionization, is comparable to that in their associated weak molecular outflows. Hence, jets also appears dynamically able to drive molecular outflows in the Class I stage. This is also true in a statistical sense: the momentum supply rate is $\simeq 100 L_{bol}/c$ in both Class I optical jets (Fig. 12(right)) and Class I molecular outflows (Fig. 14(left)).

7 Evidence for a wider-angle component

7.1 Opening angles of evolved molecular outflows

While jets in YSOs have enough *axial momentum* to drive the associated molecular outflows, the question remains whether they can reproduce the large widths and opening angles of evolved CO outflows, or whether a wider angle component is required. Interferometric observations suggest that the full opening angle at the base of molecular flows increases over time, from typical values $\leq 30^o$ in Class 0 sources (e.g. Gueth & Guilloteau 1999), to 90^o in L 1551 (Bachiller & Tafalla 1999), and up to 120^o-180^o in the old B5 outflow, of age 10^6 yrs (Velusamy & Langer 1998). Similarly broad infrared reflection nebulae are imaged around Class I and Class II jet-driving sources (Eisloeffel & Mundt 1998; Reipurth et al. 2000b).

The collimation and kinematics of Class 0 outflows are well reproduced by jet bowshocks (see Smith et al. 1997; Cabrit, Raga, Gueth 1997; Völker et al. 1999). Specific models for HH 211 are shown in Fig. 12 of Gueth & Guilloteau (1999) and Fig. 4 of Cabrit, Raga, Gueth (1997). However, because bowshocks expand faster along the jet axis than perpendicular to it ($R \propto L^{1/3}$; Wilkin 1996), collimation should increase over time, instead of the observed decrease.

Cabrit, Raga & Gueth (1997) review several effects that help avoid extreme collimation in old jet-driven CO flows: (1) the jet eventually breaks out of the molecular cloud, so the CO outflow size underestimates the jet true length (this is definitely the case in HH 111; Cernicharo & Reipurth 1996). (2) bowshocks widen with distance, following the increase of effective jet radius due to sideways ejection of material from internal surfaces, growth of a viscous mixing layer, and/or precession (see e.g. Völker et al. 1999). While both of these effects are definitely at work, none seems able to explain the very wide opening angles *at the outflow base* in some old Class I. In particular, extreme precession seems ruled out by the general excellent alignement of jet and outflow axes.

Hence it might be that a wider angle wind component is present around the bright jet beam. The wide component needs not contribute a dominant fraction of the total mass-loss rate and momentum injected along the flow axis (which are already accounted for by the jet), but it must be able to slowly push aside a broad cavity in the surrounding molecular core. Note that the cavity created by this component may be asymmetric, since the molecular outflow from DG Tau B (an evolved Class I with little envelope mass) shows a remarkably narrow redshifted lobe that does not open out until 1000 AU from the star (Mitchell et al. 1997).

7.2 Searches for wide atomic winds in HI and [O I]

Searches for a wide wind component have been conducted in the 21cm line of atomic hydrogen. Faint high-velocity wings up to $\pm$ 150 km s^{-1} were detected towards several flows in a large

beam (e.g. Lizano et al. 1988). However, subsequent imaging with the VLA shows that H I emission at $\pm$ 40 km s^{-1} is highly collimated, or even not resolved transversally. In L1551 for example, the redshifted H I is modelled as a decelerating wind with semi opening angle 20^o (Giovanardi et al. 2001), insufficient to explain the opening angle of 90^o at the base of the CO flow. A wider component is resolved at 20 km s^{-1} in the redshifted lobe of HH 7-11 (Rodriguez et al. 1990), suggesting that the wide-angle atomic wind, if it exists, is quite slow.

Recently, studies in [O I] lines have yielded two independent indications for a slow, wide flow component in T Tauri stars. The first one is the compact, very low velocity component detected in [O I]λ6300 and [O I]λ5577 towards all accreting stars: Its line profile exhibits broad wings out to $\pm$ 100 km s^{-1} and a single peak, which are best explained by keplerian rotation and a small constant vertical motion of a few km s^{-1}, i.e. a **disk wind** (Kwan & Tademaru 1995). Emission would span a range of disk radii of $R_{\rm min} = 0.1 \sin^2 i$ AU to $R_{\rm max} = 30 \sin^2 i$ AU, where i is the inclination of the disk axis to the line of sight (Hartigan et al. 1995). Assuming $i = 60^0$, and a density decreasing as $1/R^2$, one would estimate a mass outflow rate $\dot{M}_w = V_z m_H n_H(R_{\rm min}) 2\pi R_{\rm min}^2 \ln(R_{\rm max}/R_{\rm min}) \simeq 10^{-11}\ (1/x_{\rm e})(V_z/10{\rm km\ s}^{-1})(n_{\rm e}/10^7{\rm cm}^{-3})\ M_\odot{\rm yr}^{-1}$. If $x_{\rm e} \leq 10^{-2}$, the mass-loss rate in the disk wind would exceed that in the high-velocity microjet; but due to its low velocity, the ejected momentum and mechanical luminosity would not be significantly increased.

The second piece of evidence is the detection of a low-velocity [O I]λ6300 halo extending far from the microjet beam in DG Tau (Lavalley et al. 1997; Lavalley-Fouquet et al. 2000). HST spectroimaging shows that emission at $<$ 20 km s^{-1} extends to at least $\pm$ 35 AU from the jet axis at 30 AU from the star (Bacciotti et al. 2000), which corresponds to a full opening angle $\geq 90^o$. While a shocked jet cocoon cannot be excluded, the wide opening angle and the low-velocities are also compatible with the disk wind invoked above.

8 Conclusions and open questions

Several fundamental properties of jets turn out to be surprisingly similar in the various evolutionary stages of young stars, suggesting universal properties of the underlying ejection mechanism:

- The jet width appears similar in different tracers; it expands rapidly near the source, from $\leq$ 6 AU at 10 AU to $\simeq$ 30 AU at 35-50 AU, and increases slowly thereafter with an opening angle of a few degrees (compatible with sonic sideways expansion).

- The jet density increases steeply towards the central source in both optical and molecular tracers. At a distance of 30 AU, $n_{\rm H} \simeq 10^5 - 10^6$ cm^{-3} in optical Class II microjets (HH 30, DG Tau) and in molecular Class 0 jets (L 1448). On larger scale, typical densities are $n_{\rm H} \simeq 10^3 - 10^4$ cm^{-3} in optical jets, while molecular bullets reach 10^5 cm^{-3} in the shocked gas.

- The same main variability timescales are apparent: one of 500-1000 yrs (spacing between major Herbig-Haro bowshocks or molecular bullets) and a shorter one of 10-30 yrs (jet knots). Internal shocks induced by this short-term velocity variability are the main source of heating in optical jets studied so far.

- The good agreement of optical line ratios with hydrodynamical shock models in Class II and Class I optical jet knots sets an upper limit of 1 mG on the transverse field component at a distance of 150 AU (DG Tau) to 10,000 AU (HH 111) from the source. No toroidal velocity component greater than 30 km s^{-1} has been detected so far in the jets.

- Ejection is correlated with accretion signatures in all three evolutionary stages with an ejection-accretion ratio ($\dot{M}_j/\dot{M}_{\rm acc}$) $\simeq$ 0.1 (although there is a large scatter in Class II jets). The jet mechanical luminosity is $\geq 0.1 L_{\rm acc}$ in Class I and II sources, and is close to $L_{\rm acc}$ in low-luminosity Class 0 sources.

- There is mounting evidence for a slow, atomic wide-angle flow component of velocity $\leq$ 20 km s^{-1} in both Class 0 sources (HH 7-11) and Class II sources ([O I] disk wind in T Tauri stars). Mass-flux in the disk wind might exceed that in the fast jet if its ionization is very low. A sheath of intermediate velocity gas at $\simeq$ 70 km s^{-1} is traced around the fast jet beam in both Class I and Class II optical jets (HH 47; DG Tau).

Several questions that have crucial bearing on the issue of jet formation still await a definitive answer:

- What is the origin of molecules in jets and bullets in Class 0 sources ? Observations of HH 111 suggest that the molecules originate from close to the central source: the CO bullet mass seems too large for entrainment of diffuse ambient gas (Hatchell et al. 1999) and a faint molecular counterpart to the optical jet, of mass 0.0006 $M_\odot$, is found in CO spectra integrated over 60″ from the source (Cernicharo & Reipurth 1996). The resulting mass-loss rate of 10^{-6} $M_\odot$yr^{-1} is a factor of 2 higher than that inferred from optical lines. Is this molecular jet material ejected from the outer cold regions of the accretion disk, or is it entrained from the circumstellar infalling envelope into the jet by shocks/turbulent eddies ? Higher resolution observations will be required to answer this question.

- What are binarity statistics among jet sources, and how are jet properties affected ? If jet knots trace tidally induced, periodic outbursts in an excentric binary system (Reipurth 2000), the knot timescale of 10-30 years would correspond to orbital separations of 3-10 AU, which could be resolved with future instrumentation. In single stars, absence of internal shocks excited by variability would make the jets much fainter, possibly explaining the large scatter in the $\dot{M}_j$ vs $\dot{M}_{\rm acc}$ plot. While in tighter binary system, tidal truncation of the disk regions involved in the ejection might considerably alter jet properties, or even suppress jet formation. Direct constraints on the jet origin could thus be obtained by comparing jet properties in binary systems of various separations.

References

André, P. 1997, in IAU Symp. No. 182 *Herbig-Haro flows and the birth of low mass stars* eds. B. Reipurth and C. Bertout (Dordrecht: Kluwer) p. 483

Anglada, G. 1996, in Radio emission from the stars and the sun. ASP Conf Series, Vol. 93 eds. A. R. Taylor and J. M. Paredes, p.3

Anglada, G., Rodriguez, L.F., Cantó, J., Estalella, R., Torrelles, J.M. 1992, ApJ 395, 494

Anglada, G., Villuendas, E., Estallela, R., Beltrán, M.T., Rodriguez, L.F., Torrelles, J.M., Curiel, S. 1998, AJ 116, 2953

Appenzeller, I., Jancovics, I., Ostreiker, R. 1984, A&A 141, 108

Bacciotti, F., Chiuderi, C., Oliva, E. 1995, A&A 296, 185

Bacciotti, F., Eisloeffel, J. 1999, A&A 342, 717

Bacciotti, F., Eisloeffel, J., Ray, T. P. 1999, A&A 350, 917

Bacciotti, F., Mundt, R., Ray, T. P., Eisloeffel, J., Solf, J., Camezind, M. 2000, ApJ 537, L49

Bachiller, R., Tafalla, M. 1999, in The Origin of Stars and Planetary Systems. Edited by Charles J. Lada and Nikolaos D. Kylafis. Kluwer Academic Publishers, p.227

Bachiller, R., Martin-Pintado, J., Fuente, A. 1991a, A&A 243, L21

Bachiller, R., Martin-Pintado, J., Planesas, P. 1991b, A&A 251, 639

Bachiller, R., Martin-Pintado, J., Tafalla, M., Cernicharo, J., Lazareff, B. 1990, A&A 231, 174

Bachiller, R., Gueth, F., Guilloteau, S., Tafalla, M., Dutrey, A. 2000, A&A 362, L33

Bally, J., Lada, E.A., Lane, A.P. 1993, ApJ 418, 322

Bieging, J.H., Cohen, M., Schwartz, P.R. 1984, ApJ, 282, 699

Binette, L., Cabrit, S., Raga, A.C., Cantó, J. 1999, A&A 346, 260

Bontemps, S., Andre, P., Terebey, S., Cabrit, S. 1996, A&A 311, 858

Buckle, J. V., Hatchell, J., Fuller, G. A 1999, A&A 348, 584

Cabrit, S., Bertout, C. 1990, ApJ, 348, 530

Cabrit, S., Bertout, C. 1992, A&A, 261, 274

Cabrit, S., Raga, A. 2000, A&A 354, 667

Cabrit, S., Raga, A., Gueth, F. 1997, in IAU Symp. No. 182 *Herbig-Haro flows and the birth of low mass stars* eds. B. Reipurth and C. Bertout (Dordrecht: Kluwer) p.163

Cabrit, S., Edwards, S., Strom, S.E., Strom, K.M. 1990, ApJ 354, 687

Cabrit, S., et al. 1999, *The Universe as seen by ISO*, eds P. Cox et M.F. Kessler (Publisher: ESA), p.449

Ceccarelli, C., Haas, M.R., Hollenbach, D.J., Rudolph, A.L. 1997, ApJ 476, 771

Cernicharo, J., Reipurth, B. 1996, ApJ 460, L57

Cesaroni, R., Felli, M., Jenness, T., Neri, R., Olmi, L., Robberto, M., Testi, L., Walmsley, C. M. 1999A&A 345, 949

Chandler, C.J., Richer, J.S. 2001, ApJ 555, 139

Chernin, L.M. 1995, ApJ 440, L97

Claussen, M.J., Marvel, K.B., Wootten, A., Wilking, B.A. 1998, ApJ 507, L79

Cohen, M., Emerson, J.P., Beichman, C.A. 1989, ApJ 339, 455

Cohen, M., Hollenbach, D.J., Haas, M.R., Erickson, E.F. 1988, ApJ 329, 863

Corcoran, M., Ray , T.P. 1998a, A&A, 336, 535

Corcoran, M., Ray , T.P. 1998b, A&A, 331, 147

Curiel, S., Raymond, J.C., Rodriguez, L.F., Canto, J., Moran, J.M. 1990, ApJ 365, L85

Devine, D., Bally, J., Reipurth, B., Heathcote, S. 1997, AJ 114, 2095

Dougados, C., Cabrit, S., Lavalley-Fouquet, C., Ménard, F. 2000, A&A 357, L61

Downes, T.P., Ray, T.P. 1999, A&A 345, 977

Dyson, J. 1984, Ap&SS 106, 181

Edwards, S., Cabrit, S., Strom, S.E., Heyer, I., Strom, K.M., Anderson, E. 1987, ApJ 321, 473

Eisloeffel, J., Mundt, R. 1992, A&A 263, 292

Eisloeffel, J., Mundt, R. 1998, AJ 115, 1554

Eisloeffel, J., Mundt, R., Ray, T.P., Rodriguez, L.F. 2001, in *Protostars and Planets IV* (Tucson: University of Arizona Press, eds Mannings, V., Boss, A.P., Russell, S. S.), p. 815

Froebrich, D., Smith, M.D., Eisloeffel, J. 2002, submitted

Furuya, R.S., Kitamura, Y., Saito, M.,Kawabe, R., Wootten, H.A. 1999, ApJ 525, 821

Furuya, R.S., Kitamura, Y., Wootten, H.A., Claussen, M.J., Kawabe, R. 2001, ApJ 559, L143

Garcia, P., Ferreira, J., Cabrit, S., Binette, L. 2001a, A&A 377, 589

Garcia, P., Cabrit, S., Ferreira, J., Binette, L. 2001b, A&A 377, 609

Genzel, R. 1991, in *The Physics of Star formation and early stellar evolution*, eds. C.J. Lada and N.D. Kylafis (Dordrecht: Kluwer), NATO Science Series Vol. 342, p. 155

Giovanardi, C., Rodrguez, L. F., Lizano, S., Cant, J. 2000, ApJ 538, 728

Gouveia Dal Pino, E.M. 2001, ApJ 551, 347

Gredel, R. 1994, A&A 292, 580

Gueth, F. 1997, Ph.D. Thesis, Université Joseph-Fourier, Grenoble.

Gueth, F., Guilloteau, S. 1999, A&A 343, 571

Guilloteau, S., Bachiller, R., Fuente, A., Lucas, R. 1992, A&A 265, L49

Gullbring, E., Hartmann, L., Briceño, C., Calvet, N. 1998, ApJ 492, 323

Hartigan, P., Morse, J., Raymond,. J. 1994, ApJ 436, 125

Hartigan, P., Edwards, S., Gandhour, L. 1995, ApJ 452, 736

Hartigan, P., Morse, J., Heathcote, S., Cecil, G., Raymond, J. 1993, ApJ 414, L121

Hartigan, P., Bally, J., Reipurth, B., Morse, J. A. 2000, in *Protostars and Planets IV* (Tucson: University of Arizona Press, eds Mannings, V., Boss, A.P., Russell, S. S.), p. 841

Hartigan, P., Morse, J.A., Reipurth, B., Heathcote, S., Bally, J. 2001, ApJ 559, L157

Hatchell, J., Fuller, G. A., Ladd, E. F. 1999, A&A 346, 278

Heathcote, S., Reipurth, B. 1992, AJ 104, 2193

Henriksen, R., Andre, P., Bontemps, S. 1997, A&A 323, 549

Hester, J.J., Stapelfeldt, K.R., Scowen, P.A. 1998, AJ 116, 372

Hirth, G.A., Mundt, R., Solf, J. 1995, ApJ 427, L99

Hirth, G.A., Mundt, R., Solf, J. 1997, A&ASS 126, 437

Hollenbach, D.J. 1997, in IAU Symp. No. 182 *Herbig-Haro flows and the birth of low mass stars* eds. B. Reipurth and C. Bertout (Dordrecht: Kluwer) p. 181

Hollenbach, D., McKee, C.F. 1989, ApJ 342,306

Kwan, J., Tademaru, E. 1995, ApJ 454, 382

Lada, C.J. 1985, ARAA, 23, 267

Lavalley, C. 2000, Ph.D. Thesis, Université Joseph Fourier, Grenoble, France.

Lavalley, C., Cabrit, S., Dougados, C., Ferruit, P., Bacon, R. 1997 A&A 327, 671

Lavalley-Fouquet, C., Cabrit, S., Dougados, C. 2000, A&A, 356, L41

Liseau, R. et al. 1996, A&A 315, L181

Liseau, R. et al. 1997, in IAU Symp. No. 182 *Herbig-Haro flows and the birth of low mass stars* eds. B. Reipurth and C. Bertout (Dordrecht: Kluwer) p. 111

Lizano, S., Torrelles, J.M., eds. 1995 RMxAA, Serie de conferencias, Vol. 1

Lizano, S., Heiles, C., Rodriguez, L.F., Koo, B.-C., Shu, F.H., Hasegawa, T., Hayashi, S., Mirabel, I. F. 1988, ApJ 328, 763

McCaughrean, M. J., Rayner, J. T., Zinnecker, H 1994, ApJ 436, L189

Marti, J., Rodriguez, L. F., Reipurth, B. 1993, ApJ 416, 208

Marti, J., Rodriguez, L. F., Reipurth, B. 1995, ApJ 449, 184

Marti, J., Rodriguez, L.F., Reipurth, B. 1998, ApJ 502, 337

Martin-Pintado, J., Bachiller, R., Fuente, A. 1992, A&A 254, 315

Mitchell, G.F., Sargent, A.I., Mannings, V. 1997, ApJ 483, L127

Mundt, R. 1992, in *Stellar jets and bipolar outflows*, eds. L. Errico and A.A. Vittone (Dordrecht: Kluwer), p.91

Mundt, R., Fried, J.W. 1983, ApJ, 274, L83

Mundt, R., Ray, T.P. 1994, in *The Nature and Evolutionary Status of Herbig Ae/Be stars*, ASP Conf. Ser. 62 (San Francisco: ASP), p. 237

Mundt, R., Brugel, E.W., Bührke, T. 1987, ApJ 319, 275

Mundt, R., Ray, T.P., Raga, A.C. 1991, A&A 252, 740

Nisini, B., Benedettini, M., Giannini, T., Codella, C., Lorenzetti, di Giorgio, A. M., Richer, J. S. 2000, A&A 360, 297

Osterbrock, D. 1989, *Astrophysics of gaseous nebulae and active galactic nuclei* (Mill Valley, University Science Books)

Panagia, N. 1991, in *The Physics of Star formation and early stellar evolution*, eds. C.J. Lada and N.D. Kylafis (Dordrecht: Kluwer), NATO Science Series Vol. 342, p. 565

Pineau des Forêts, G., Flower, D.R., Chièze, J.-P. 1997, in IAU Symp. No. 182 *Herbig-Haro flows and the birth of low mass stars* eds. B. Reipurth and C. Bertout (Dordrecht: Kluwer) p. 199

Raga, A. C., Kofman, Lev 1992, ApJ 386, 222

Raga, A. C., Biro, S. 1993, MNRAS 264, 758

Raga, A.C., Böhm, K.H., Cantó J. 1996, RMxAA 32, 161

Raga, A.C., Noriega-Crespo, A. 1998, AJ 116, 2943

Raga, Alejandro C., Binette, L., Canto, J., Calvet, N. 1990, ApJ 364, 601

Ray, T.P., Mundt, R., Dyson, J.E., Falle, S.A.E.G., Raga, A. 1996, ApJ 468, L103

Reipurth, B. 2000, AJ 120, 3177

Reipurth, B. 2001, A general catalog of Herbig-Haro objects, `http://www.casa.colorado.edu/hhcat`.

Reipurth, B., Bertout, C., eds. 1997. *IAU Symp. No. 192: Herbig-Haro Flows and the Birth of Low Mass Stars* (Dordrecht:Kluwer)

Reipurth, B., Raga, A.C. 1999, in *The origin of stars and planetary systems*, eds. C.J. Lada and N.D. Kylafis (Dordrecht: Kluwer), NATO Science Series Vol. 540, p. 267

Reipurth, B., Bally, J. 2001, ARA&A 37, 403

Reipurth, B., Bally, J., Devine, D. 1997a, AJ 114, 2708

Reipurth, B., Hartigan, P., Heathcote, S., Morse, J. A., Bally, J. 1997b, AJ 114, 757

Reipurth, B., Bally, J., Fesen, R.A., Devine, D. 1998, Nature, 396, 343

Reipurth, B., Heathcote, S., Yu, K.C., Bally, J., Rodriguez, L.F. 2000a, ApJ 534, 317

Reipurth, B., Yu, K. C., Heathcote, S., Bally, J., Rodrguez, L. F. 2000b, AJ 120, 1449

Reynolds, S. 1986, ApJ 304, 713

Richer, J. S., Shepherd, D. S., Cabrit, S., Bachiller, R., Churchwell, E. 2000, in *Protostars and Planets IV* (Tucson: University of Arizona Press, eds Mannings, V., Boss, A.P., Russell, S. S.), p. 867

Rodriguez, L. F., Anglada, G., Raga, A. 1995, ApJ 454, L149

Rodriguez, L.F. 1995, RMxAA, Serie de conferencias, Vol. 1, p.1

Rodriguez, L.F., Escalante, V., Lizano, S., Canto, J., Mirabel, I.F., 1990, ApJ 365, 261

Rodriguez, L. F., Torrelles, J. M., Anglada, G., Marti, J. 2001, RMxAA 37, 95

Smith, M. D., Suttner, G., Yorke, H. W. 1997, A&A 323, 223

Snell, R. L., Loren, R. B., Plambeck, R. L. 1980, ApJ 239, L17

Solf, J. 1987, A&A 184, 322

Solf, J. 1989 in *ESO workshop on low mass star formation and pre-main sequence objects*, eds. B. Reipurth (Garching: ESO), p. 399

Solf, J. 1997 in *Herbig-Haro flows and the birth of low-mass stars*, IAU Symp. No. 182, eds. B. Reipurth and C. Bertout (Dordrecht: Kluwer), p. 63

Velusamy, T., Langer, W. D. 1998, Nature, 392, 685

Völker, R., Smith, M.D., Suttner, G., Yorke, H.W. 1999, A&A 343, 953

Wilkin, F. 1996, ApJ 459, L31

Zinnecker, H., McCaughrean, M. J., Rayner, J. T. 1998, Nature 394, 862